CRYSTAL GROWTH & DESIGN

Article

Cite This: Cryst. Growth Des. 2019, 19, 5292−5307

pubs.acs.org/crystal

Syntheses, Crystal Structures, Luminescent Properties, and Electrochemical Synthesis of Group 12 Element Coordination Polymers with 4-Substituted 1,2,4-Triazole Ligands

Houria Benaissa,[†] Mariusz Wolff,[†,‡] Koen Robeyns,[†] Günther Knör,[‡] Kristof Van Hecke,[§] Nicolo Campagnol,[∥] Jan Fransaer,[∥] and Yann Garcia*[,†]

[†]Université Catholique de Louvain, Institute of Condensed Matter and Nanosciences, Molecular Chemistry, Materials and Catalysis (IMCN/MOST), Place Louis Pasteur 1, 1348 Louvain-la-Neuve, Belgium

[‡]Johannes Kepler University Linz, Institute of Inorganic Chemistry, Altenbergerstraße 69, 4040 Linz, Austria

[§]XStruct, Department of Chemistry, Ghent University, Krijgslaan 281-S3, 9000 Ghent, Belgium

[∥]Department of Materials Engineering, KU Leuven, Kasteelpaark Arenberg 44, 3001 Heverlee, Belgium

Supporting Information

ABSTRACT: The self-assembly of Zn(II), Cd(II), or Hg(II) salts with long flexible 1,2,4-triazole-based ligands resulted in coordination polymers and mononuclear complexes of diverse topology. Indeed, the 1D chain $[ZnCl_2(\boldsymbol{btpm})]$ (**1**) ($P\bar{1}$), the 2D square grid $[Zn(\boldsymbol{btpm})_2(H_2O)](BF_4)_2\cdot 2\boldsymbol{btpm}\cdot 8H_2O$ (**2**) ($P2_12_12$), and the 1D chain $[Cd_3Cl_6(\boldsymbol{btpm})_2]\cdot 8H_2O$ (**3**) ($P\bar{1}$) with ***btpm*** = bis(4-(1,2,4-triazol-4-yl)phenyl)methane were crystallized. In addition, the mononuclear complexes $[ZnCl_2(\boldsymbol{ppt})_2]$ (**4**) ($I2$) and $[HgBr_2(\boldsymbol{ppt})_2]$ (**5**) ($C2$) were obtained along with the 1D polymer $[Cd_2Cl_2(\boldsymbol{ppt})_4](CdCl_4)\cdot 4DMF$ (**6**) ($P1$) with ***ppt*** = (4-phenoxyphenyl)-1,2,4-triazole. 1D chains of the formula $[ZnCl_2(\boldsymbol{tpca})]$ (**7**) ($P2_1/c$) and $[HgBr_2(\boldsymbol{tpca})]$ (**8**) ($P2_1/c$) along with the 2D net $[Cd(\boldsymbol{tpca})_2(H_2O)_2]\cdot 2H_2O$ ($C2/c$) (**9**) with ***tpca*** = *N*-(1,2,4-triazol-4-yl)pyridine-3-carboxamide were obtained. In addition, the X-ray structures of ***tpca*** and ***ppt*** are described. All compounds display solid-state blue luminescence, which has been investigated in detail. Electrochemical synthesis of **2**, which has been rarely applied for MOF synthesis, revealed hollow particles.

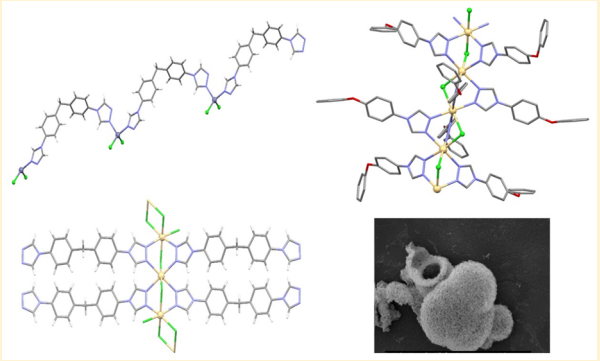

1. INTRODUCTION

Azoles and their derivatives are widely used as organic connectors in supramolecular coordination chemistry, leading to a variety of networks due to their numerous coordination modes.[1−7] This includes monodentate, bidentate chelating, or bidentate bridging modes, depending on the position and the nature of the substituent at the azole ring. The types of architecture range from 1D azole coordination polymers (ACPs) to 2D or 3D metal-azolate networks (MANs) and frameworks (MAFs).[8−18] It is quite challenging to control the construction of polynuclear complexes, as structural modifications of building blocks influence the final structural motifs through covalent bonding and various weak interactions. Therefore, the selection of organic connectors with proper length, flexibility, and symmetry is critical to obtain special topology structures. The development of new organic connectors is, and will remain, an important aspect in supramolecular coordination chemistry.

ACPs, MANs, and MAFs have attracted considerable attention due to their fascinating architectures and topologies and their possible application in various areas such as catalysis,[19] chiral resolution,[20] gas storage,[21] luminescence,[22,23] magnetism,[24] medicine,[25] spin crossover,[26,27] etc.

1,2,4-Triazole and, in particular, its derivatives were used to tailor polynuclear complexes, including dinuclear, linear trinuclear, cyclic trinuclear, and hexanuclear ring complexes, to name a few.[1] Only a few examples that use "long" flexible 1,2,4-triazole derivative ligands for the construction of MANs and MAFs have been reported, however.[28−32] Our laboratory is currently exploiting the potential of a transamination reaction to produce such molecules and build coordination polymers.[33] In order to investigate the influence of the length and flexibility of the ligand and the synthesis conditions on the architecture and luminescence properties of coordination polymers (CPs) and complexes, eight zinc, cadmium, and mercury derivatives of such compounds were prepared: namely, $[ZnCl_2(\boldsymbol{btpm})]$ (**1**), $[Zn(\boldsymbol{btpm})_2(H_2O)](BF_4)_2\cdot 2\boldsymbol{btpm}\cdot 8H_2O$ (**2**), $[Cd_3Cl_6(\boldsymbol{btpm})_2]\cdot 8H_2O$ (**3**) with ***btpm*** = bis(4-(1,2,4-triazol-

Received: June 9, 2019
Revised: July 24, 2019
Published: August 12, 2019

DOI: 10.1021/acs.cgd.9b00734
Cryst. Growth Des. 2019, 19, 5292−5307

Table 1. Crystallographic Data for 1−9, *tpca*, and *ppt*

	1	2	3	4	5
CCDC no.	1918038	1918039	1918040	1918041	1918045
empirical formula	$C_{17}H_{14}Cl_2N_6Zn$	$C_{68}H_{68}B_2F_8N_{24}O_{9.32}Zn$	$C_{34}H_{28}Cd_3Cl_6N_{12}O_8$	$C_{84}H_{66}Cl_6N_{18}O_6Zn_3$	$C_{28}H_{22}Br_2HgN_6O_2$
formula wt	438.61	1609.49	1282.58	1832.35	834.92
temp (K)	150(2)	150(2)	150(2)	296(2)	297(2)
wavelength (Å)	0.71073	0.71073	0.71073	0.71073	0.71073
cryst syst	triclinic	orthorhombic	monoclinic	monoclinic	monoclinic
space group	$P\bar{1}$	$P2_12_12$	$P2_1/c$	$I2$	$C2$
unit cell dimens					
a (Å)	8.886(7)	20.6690(5)	11.0651(4)	14.1345(10)	16.7185(8)
b (Å)	8.972(9)	22.1447(5)	14.3431(6)	5.9976(5)	6.0491(2)
c (Å)	12.207(8)	8.5068(2)	17.6239(5)	48.638(4)	13.8547(6)
α (deg)	74.58(8)	90	90	90	90
β (deg)	79.59(7)	90	96.973(3)	96.509(7)°	99.057(4)
γ (deg)	68.31(8)	90	90	90	90
V (Å^3)	868.0(14)	3893.62(16)	2776.36(18)	4096.6(5)	1383.70(10)
Z	2	2	2	2	2
calcd density (Mg/m^3)	1.678	1.373	1.534	1.485	2.004
abs coeff (mm^{-1})	1.737	0.405	1.478	1.133	8.487
F(000)	444	1661	1252	1872	796
cryst size (mm^3)	0.15 × 0.14 × 0.03	0.25 × 0.15 × 0.10	0.08 × 0.06 × 0.05	0.40 × 0.25 × 0.12	0.40 × 0.14 × 0.07
θ range (deg)	2.863−20.811	2.930−25.505	3.070−25.243	2.901−25.243	3.556−25.687
no. of rflns collected	6269	24175	19735	12516	7989
no. of indep rflns	1791 (R_{int} = 0.2284)	7226 (R_{int} = 0.0477)	5009 (R_{int} = 0.0610)	7158 (R_{int} = 0.0607)	2594 (R_{int} = 0.0442)
completeness (%)	99.3, θ = 20.811°	99.7, θ = 25.242°	99.7, θ = 25.242°	99.3, θ = 25.242°	98.8, θ = 25.242°
max, min transmission	1, 0.136	1, 0.897	1, 0.62771	1, 0.571	1, 0.314
refinement method	full-matrix least squares on F^2	full-matrix least squares on F^2	full-matrix least squares on F^2	full-matrix least squares on F^2	full-matrix least squares on F^2
no. of data/restraints/params	1791/0/235	7226/48/564	5009/0/312	7158/256/713	2594/13/153
GOF	1.022	1.046	1.097	1.008	1.029
final R indices ($I > 2\sigma(I)$)	R1 = 0.0793, wR2 = 0.1723	R1 = 0.0515, wR2 = 0.1408	R1 = 0.0610, wR2 = 0.1538	R1 = 0.0583, wR2 = 0.1538	R1 = 0.0322, wR2 = 0.0851
R indices (all data)	R1 = 0.1037, wR2 = 0.1822	R1 = 0.0587, wR2 = 0.1474	R1 = 0.0777, wR2 = 0.1625	R1 = 0.0718, wR2 = 0.1644	R1 = 0.0328, wR2 = 0.0858
$\Delta\rho$ max/min (e Å^{-3})	1.127/−0.891	1.402/−0.373	3.172/−0.995	0.669/−0.511	0.737/−0.655
Flack param		0.015(6)		−0.007(15)	−0.015(9)

	6	7	8	9	*tpca*	*ppt*
CCDC no.	1918042	1918043	1918046	1918044	1918047	1920056
empirical formula	$C_{68}H_{72}Cd_3Cl_6N_{16}O_8$	$C_8H_7Cl_2N_5OZn$	$C_8H_7Br_2HgN_5O$	$C_{16}H_{20}CdN_{10}O_6$	$C_8H_7N_5O$	$C_{14}H_{11}N_3O$
formula wt	1791.31	325.46	549.60	560.82	189.19	237.26
temp (K)	150(2)	296(2)	297(2)	296(2)	297(2)	100.0(1)
wavelength (Å)	0.71073	0.71073	0.71073	0.71073	0.71073	1.54184
cryst syst	triclinic	monoclinic	monoclinic	monoclinic	monoclinic	monoclinic
space group	$P\bar{1}$	$P2_1/c$	$P2_1/c$	$C2/c$	$I2/a$	$P2_1/n$
unit cell dimens						
a (Å)	14.0170(11)	7.65057(10)	7.9205(5)	15.4173(9)	13.856(3)	9.1614(6)
b (Å)	15.1792(11)	16.9157(2)	17.8180(9)	8.0479(4)	8.7855(10)	14.5345(6)
c (Å)	19.0504(13)	9.11073(13)	9.3333(5)	16.5561(9)	14.985(3)	9.5198(6)
α (deg)	97.428(6)	90	90	90	90	90
β (deg)	99.063(6)	99.2148(13)	99.132(6)	90.567(5)	108.00(2)	115.558(8)
γ (deg)	108.061(7)	90	90	90	90	90
V (Å^3)	3736.3(5)	1163.85(3)	1300.49(13)	2054.12(19)	1734.8(5)	1143.57(13)
Z	2	4	4	4	8	4
calcd density (Mg/m^3)	1.592	1.857	2.807	1.813	1.449	1.378
abs coeff (mm^{-1})	1.125	2.558	17.971	1.123	0.105	0.731
F(000)	1804	648	992	1128	784	496
cryst size (mm^3)	0.50 × 0.10 × 0.02	0.60 × 0.10 × 0.05	0.35 × 0.30 × 0.06	0.30 × 0.20 × 0.15	0.50 × 0.30 × 0.30	0.194 × 0.154 × 0.102
θ range (deg)	2.771−25.257	3.450−26.188	3.340−25.534	3.104−26.212	3.635−26.041	5.603−75.502
no. of rflns collected	14949	13489	8911	8925	2902	10988
no. of indep rflns	14949 (R_{int} = /)[a]	2307 (R_{int} = 0.0336)	2373 (R_{int} = 0.0541)	2034 (R_{int} = 0.0284)	2902 (R_{int} = /)[a]	2311 (R_{int} = 0.0497)

DOI: 10.1021/acs.cgd.9b00734
Cryst. Growth Des. 2019, 19, 5292−5307

Table 1. continued

	6	7	8	9	*tpca*	*ppt*
completeness (%)	96.5, θ = 25.242°	99.0,θ = 25.242°	97.8, θ = 25.242°	99.1, θ = 25.242°	98.2, θ = 25.242°	99.9, θ = 67.684°
max, min transmission	1, 0.495	1 , 0.700	1, 0.119	1, 0.849	1, 0.754	0.955, 0.931
refinement method	full-matrix least squares on F^2	full-matrix least squares on F^2	full-matrix least squares on F^2	full-matrix least squares on F^2	full-matrix least squares on F^2	full-matrix least squares on F^2
no. of data/ restraints/ params	14949/282/840	2307/0/154	2373/0/154	2034/0/157	2902/0/128	2311/0/163
GOF	1.095	1.044	1.098	1.081	1.057	1.061
final R indices ($I > 2\sigma(I)$)	R1 = 0.0732, wR2 = 0.1795	R1 = 0.0252, wR2 = 0.0634	R1 = 0.0637, wR2 = 0.1779	R1 = 0.0217, wR2 = 0.0559	R1 = 0.0726, wR2 = 0.1728	R1 = 0.0475, wR2 = 0.1236
R indices (all data)	R1 = 0.1009, wR2 = 0.1952	R1 = 0.0267, wR2 = 0.0640	R1 = 0.0677, wR2 = 0.1826	R1 = 0.0231, wR2 = 0.0571	R1 = 0.0841, wR2 = 0.1798	R1 = 0.0531, wR2 = 0.1316
$\Delta\rho$ max/min (e Å^{-3})	1.535 and −1.470	0.376 and −0.239	3.099/−1.252	0.326/−0.301	0.187/−0.183	0.218/−0.353

[a]Twinned data set, refined against unmerged HKLF 5 formatted reflections.

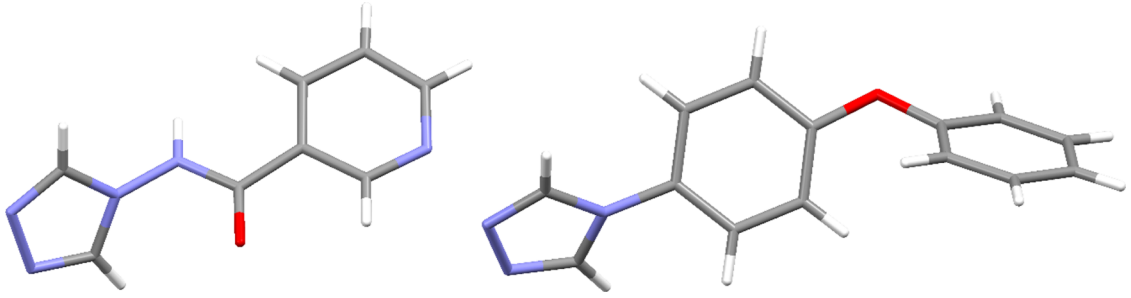

Figure 1. Stick representations of ***tpca*** (left) and ***ppt*** (right).

Scheme 1. Views of *btpm*, *tpca*, and *ppt*

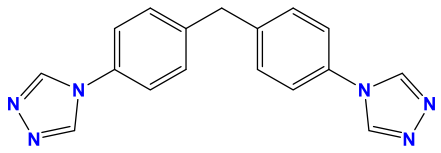

bis(4-(1,2,4-triazol-4-yl)phenyl)methane (***btpm***)

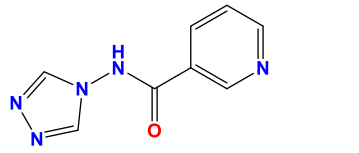

N-(1,2,4-triazol-4-yl)pyridine-3-carboxamide (***tpca***)

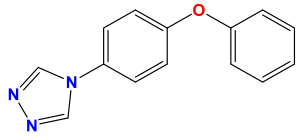

1-(4-phenoxyphenyl)-1,3,4-triazole (***ppt***)

4-yl)phenyl)methane, $[ZnCl_2(ppt)_2]$ (**4**), $[HgBr_2(ppt)_2]$ (**5**), and $[Cd_2Cl_2(ppt)_4](CdCl_4)\cdot 4DMF$ (**6**) with ***ppt*** = (4-phenoxyphenyl)-1,3,4-triazole, and $[ZnCl_2(tpca)]$ (**7**), $[HgBr_2(tpca)]$ (**8**), and $[Cd(tpca)_2(H_2O)_2]\cdot 2H_2O$ (**9**) with ***tpca*** = *N*-(1,2,4-triazol-4-yl)pyridine-3-carboxamide. In addition, the X-ray structures of ***tpca*** and ***ppt***, as well as all complexes, were determined by single-crystal X-ray diffraction and the compounds were further characterized by elemental analyses, MS, NMR, and FT-IR spectroscopy. Their luminescence properties were also investigated along with the possibility of preparing such compounds by electrochemical synthesis, which has been infrequently applied in this field. Luminescence studies are motivated by recent pioneering works which demonstrated the interplay between spin crossover phenomena and fluorescence properties of coordination complexes including 1,2,4-triazole ligands.[34−36]

2. RESULTS

2.1. Syntheses. The ***btpm*** molecule was prepared according to the procedure we previously described.[33] ***tpca*** and ***ppt*** were prepared via transamination, from nicotinic hydrazide and 4-phenoxyaniline, respectively. Both molecules were prepared as single crystals suitable for X-ray diffraction. Crystal formation of the complexes was initially attempted by slow diffusion in MeOH because our ligands and metallic salts are both readily soluble in this solvent. This procedure led to powders which were recrystallized, leading to single crystals for **1** and **2**. Solvothermal (with DMF) or hydrothermal conditions, followed by slow evaporation, led to single crystals for **3**, **4**, **6**, **9**, and **7**, respectively. **5** and **8** were obtained by slow evaporation of the reactants. All complexes were investigated by FT-IR (Figure S1), thermogravimetric analyses (Figure S2), and CHN analyses as well as by single-crystal X-ray diffraction. Indeed, nine crystal structures of coordination complexes were obtained.

DOI: 10.1021/acs.cgd.9b00734
Cryst. Growth Des. 2019, 19, 5292−5307

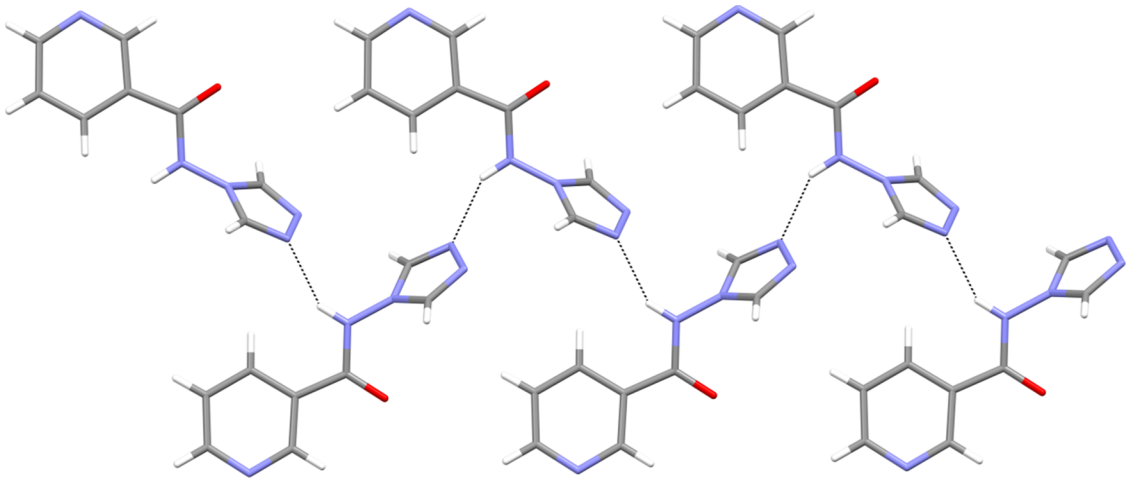

Figure 2. Hydrogen bond patterns as observed in the crystal packing of ***tpca***.

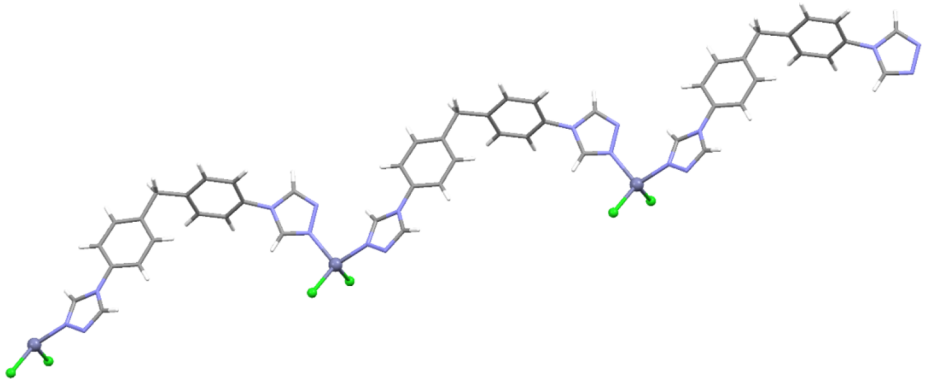

Figure 3. Extended view of **1** showing three consecutive moieties of [$ZnCl_2$(***btpm***)]. Formula units are arranged in 1D coordination chains with tetrahedral geometries around the Zn(II) cation.

For completeness, the crystal structures of ***tcpa*** and ***ppt*** are also presented.

2.2. Crystal Structures. In the following, we present crystal structures of the molecules ***tpca*** and ***ppt*** as well as the coordination complexes **1**−**9**. Crystallographic data are given in Table 1, whereas bond lengths and bond angles are gathered in Tables S1−S9. Crystal and molecular structures are shown in Figures 1−10.

*2.2.1. Crystal Structure of N-(1,2,4-Triazol-4-yl)pyridine-3-carboxamide (**tpca**).* The ***tpca*** molecule (Scheme 1 and Figure 1) was crystallized by slow evaporation from a methanolic mother solution and afforded colorless needlelike crystals. Single-crystal analysis shows that ***tpca*** arranges itself in the *I*-centered monoclinic space group $I2/a$. In its free form, the triazole unit is rotated out of the plane formed by the rest of the molecule, by about 60°. The ***tpca*** molecules are packed into layers, stretching along the *b* axis, with hydrogen bonding between the central N−H and a triazole nitrogen (N−H···N = 2.02 Å; N···N = 2.782(4) Å; Table S10), resulting in a *zigzag* organization of molecules within this layer (Figure 2).

*2.2.2. Crystal Structure of 1-(4-Phenoxyphenyl)-1,3,4-triazole (**ppt**).* The crystal structure of ***ppt*** (Figure 1), obtained by recrystallization from MeOH, shows $P2_1/n$ symmetry. The triazole ring is angled at about 44° from the central phenyl ring, which in turn is tilted about 70° from the terminal phenyl ring. The crystal packing is stabilized by parallel displaced $\pi-\pi$ stacking interactions around the inversion center, involving the central aromatic ring system, with a perpendicular distance between the centroid of the ring and the corresponding plane of 3.3017(6) Å.

*2.2.3. Crystal Structure of [$ZnCl_2$(**btpm**)] (**1**).* CP **1** crystallizes in the triclinic space group $P\bar{1}$. Its asymmetric unit contains one Zn(II) cation, one V-shaped ***btpm*** ligand, and two chloride atoms. The Zn(II) cation is coordinated by two triazole N atoms of two bridging ***btpm*** ligands and two chloride ions (Figure 3), forming a distorted-tetrahedral ZnN_2Cl_2 geometry with a distortion parameter τ_4 of 0.88. We recall that for an ideal square-planar geometry $\tau_4 = 0$, while for an ideal tetrahedral geometry $\tau_4 = 1$.[37] The V-shaped ***btpm*** ligand bridges (via the coordination mode III, Scheme S1) two Zn(II) atoms to form a 1D linear polymeric chain with a Zn(1)···Zn(1) distance of 15.18(2) Å and Zn(1)···Zn(1)···Zn(1) angle of 180° (Figure 3). While the angle between the 1,2,4-triazole and phenyl ring planes is 22.1° on one side, it is 52.1° on the other. The dihedral angle between the phenyl rings is 69.7°. The CH_2 linker of the ligand angles at 116(1)°, and the dihedral angles between consecutive aromatic rings reduce the angle, resulting in a Zn−CH_2−Zn angle of 106.8(1)°.

*2.2.4. Crystal Structure of [Zn(**btpm**)$_2$(H_2O)](BF_4)$_2$·2btpm·8H_2O (**2**).* CP **2** crystallizes in the orthorhombic space group $P2_12_12$. The unit cell contains two formula units with the crystallographic 2-fold axis running though the central Zn(II) cation and the coordinated water molecule. Four bridging ***btpm*** groups are coordinated to the Zn(II) cation. The asymmetric

DOI: 10.1021/acs.cgd.9b00734
Cryst. Growth Des. 2019, 19, 5292−5307

unit contains an independent Zn(II) cation, one coordinated V-shaped ***btpm*** ligand, one uncoordinated V-shaped ***btpm*** ligand, half of a coordinated water molecule, four lattice water molecules, and one tetrafluoroborate anion. The coordination geometry around the Zn(II) cation is a distorted ZnN_4O trigonal bipyramid. Zn(1) is bonded by four N atoms from four V-shaped ***btpm*** ligands and one O atom from a water molecule.

The structure of **2** can be described as a 2D square-grid coordination polymer (along the *ab* plane) with dimensions of 15.157 × 15.157 Å and diagonal-to-diagonal Zn···Zn distances of 20.7 × 22.1 Å. It is constructed from 64-membered nonplanar rings. Each ring is built from four Zn(II) centers bridged by four ***btpm*** ligands with coordination mode III (Scheme S1). The structure of **2** affords a 2D 4-connected unimodal network with point Schläfli symbol $\{4^4.6^2\}$ and exhibits a sqlnet topology, which was determined by using the program package TopOsPro.[38]

The channels are occupied by free lattice water molecules and BF_4^- anions, and the 2D layers are placed on top of each other, forming channels along the *c* axis and sandwiched free ligands between coordinated ligands held together by C−H···π interactions between the central methylene group and phenyl rings of neighboring molecules X−π of around 3.5 Å. The structure is further stabilized by two hydrogen bonds between the coordinated water and the free ***btpm*** ligand (Figure 4), as such forming a 3D supramolecular framework. The isolated water molecules could not all be refined as fully occupied, probably due to the loose association of the CP and the possible mobility within the open channels.

The CH_2 group of the ***btpm*** ligand behaves more tetragonally, with an angle involving the pivot atoms of the connecting phenyl rings measured at 110.9(4)°. The Zn−CH_2−Zn angle follows the same trend and shows an angle of 103.53°; the free ***btpm*** ligand, less restrained by the participation in a 2D network, has a slightly wider angle around the CH_2 moiety (112.6(5)°). Searches in the CSD database reveal that the average angle is found to be 114(3)°.[39] Dihedral angles between neighboring aromatic rings are 26.80, 70.84, and 12.32° for the coordinated ligand; the triazole−phenyl dihedral angles for the uncoordinated ***btpm*** show that the consecutive rings are almost planar (0.34 and 8.21°), and the angle between the phenyl rings is comparable to that of the coordinated ***btpm*** (71.25°).

*2.2.5. Crystal Structure of [Cd_3Cl_6(**btpm**)$_2$]·8H_2O (**3**).* CP **3** crystallizes in the triclinic space group $P\bar{1}$. The asymmetric unit contains two crystallographically independent Cd(II) cations, three chloride anions, one V-shaped ***btpm*** ligand, and four lattice water molecules, one of which is found disordered over two sites. The ***btpm*** ligand exhibits a bent conformation and shows a μ_4-tetradentate coordination mode (coordination mode 1, Scheme S1) through two triazole N,N bridges. **3** is made up of linear trinuclear Cd units, interconnected by two μ_2-bridging chloride atoms to form a polymeric 1D chain along the *a* direction. In the trinuclear fragment, the central Cd(II) cation is positioned on an inversion center, coordinated by four N atoms of four ***btpm*** ligands and two chloride atoms, and links to the terminal Cd(II) cation by one μ_2-bridging chloride and two triazole *N,N*-bridging ***btpm*** ligands, separating both Cd(II) cations 3.887 Å from each other. Three chlorides (one terminal Cl atom and two bridging μ_2-Cl atoms) complete the coordination sphere of the terminal Cd(II) cation (Figure 5).

CP **3** possesses 3D interpenetrating channels amounting to about 915 Å^3 or about one-third of the unit cell. The cavities were partially filled with localized water molecules; in the main

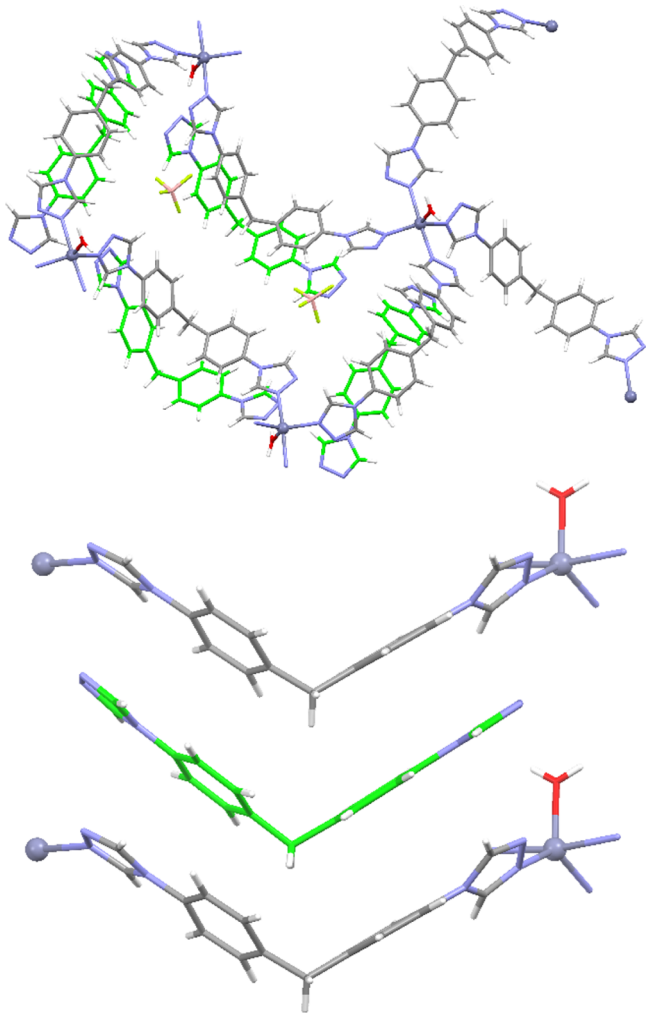

Figure 4. Partial packing diagram of **2** showing four ***btpm*** units coordinated to a central Zn atom (top) and stacking arrangement (bottom) of the 2D layers (carbon atoms in gray) and the free ***btpm*** (carbon atoms in green), stabilized by π−π interactions.

channel along the *a* direction, surrounded by the 2D polymer, a void space with disordered solvent molecules is present (204 Å^3 per channel), which was treated by the Platon Squeeze algorithm.[40] The 2D layers are connected by π−π stacking interactions between triazole and phenyl rings on both sides of the ***btpm*** ligand to form a 3D framework. The centroid−centroid distances are 3.741(5) and 3.832(5) Å, with almost parallel dihedral angles (α), 6.4(4) and 4.0(4)°, respectively. The β angles, defined as the angle between the centroid−centroid vector and the ring normal, are 23.1 and 22.6°, respectively. Slippage is 1.47 Å for both interactions. Minor full-molecule disorder is observed, which could only be modeled for the Cd_3Cl_6 unit, amounting to about 6% observed disorder.

Four Cd(II) cations are linked by four N atoms of the V-shaped ***btpm*** ligand along the *c* direction, with Cd···Cd distances of 17.624 Å. **3** forms a 2D biwave layer, as Cd(II) cations are linked by the bent ***btpm*** ligand from two directions. The CH_2 angle is stretched, 117.1(7)°. The angles between the 1,2,4-triazole and phenyl rings are 19.91 and 23.21°, and the angle between both phenyl rings is 50.34°.

The structure of **3** affords a binodal network with point Schläfli symbol $\{3^{12}.4^{14}.5^2\}\{3^6.4^6.5^3\}^2$ and exhibits a 6,8-c net topology with stoichiometry (6-c)^2(8-c). The topology of

DOI: 10.1021/acs.cgd.9b00734
Cryst. Growth Des. 2019, 19, 5292−5307

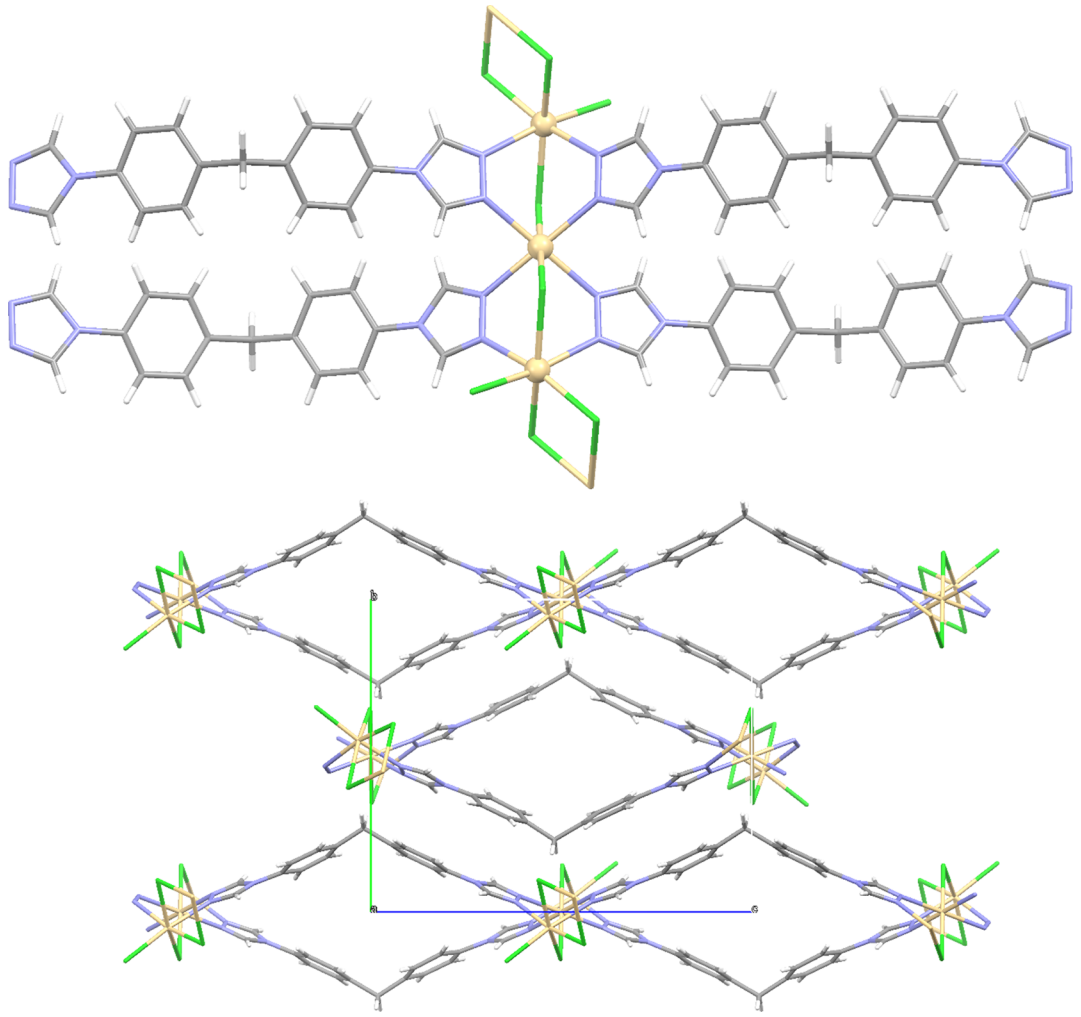

Figure 5. (top) Trinuclear Cd unit of **3** with bridging ***btpm*** ligands and Cl atoms and (bottom) 2D biwave layer of **3** along the *a* axis.

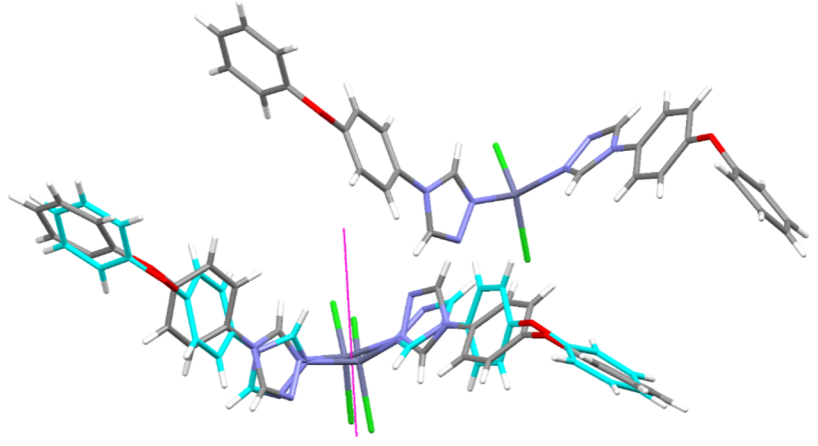

Figure 6. Stick representation of the expanded asymmetric unit of **4** showing the observed disorder of the formula unit around the 2-fold axis (indicated as a magenta line).

polymer **3** was determined using the program package ToposPro.[38]

*2.2.6. Crystal Structure of [$ZnCl_2$(**ppt**)$_2$] (**4**).* Compound **4** crystallizes in the chiral monoclinic space group *I*2, and its asymmetric unit contains one and a half [$ZnCl_2$(***ppt***)$_2$] complexes; one formula unit is found disordered around the crystallographic 2-fold axis, with the Zn(II) metal ion found in close proximity of this axis (Figure 6). The Zn(II) ion adopts a slightly distorted tetrahedral geometry, and each Zn(II) ion is coordinated by two chloride atoms and two triazole N atoms of two ***ppt*** ligands, to form a mononuclear complex.

*2.2.7. Crystal Structure of [$HgBr_2$(**ppt**)$_2$] (**5**).* **5** crystallizes in the monoclinic space group *C*2, with half a formula unit in the asymmetric unit. The crystallographic 2-fold axis generates a

DOI: 10.1021/acs.cgd.9b00734
Cryst. Growth Des. 2019, 19, 5292−5307

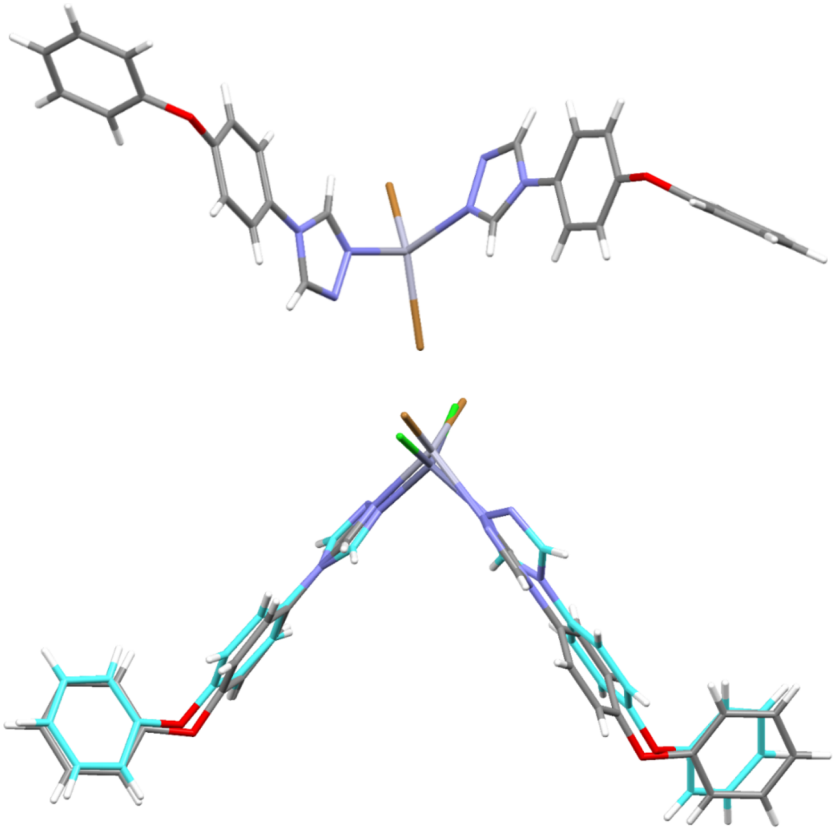

Figure 7. (top) Stick representation of **5**. Note the similar conformation in comparison to **4** in Figure 6. (bottom) Superposition of **4** and **5**, through the oxygen atoms and the metal centers. The ***ppt*** ligand on the left fits almost perfectly; the right side and the terminal phenyl groups are less isostructural, however.

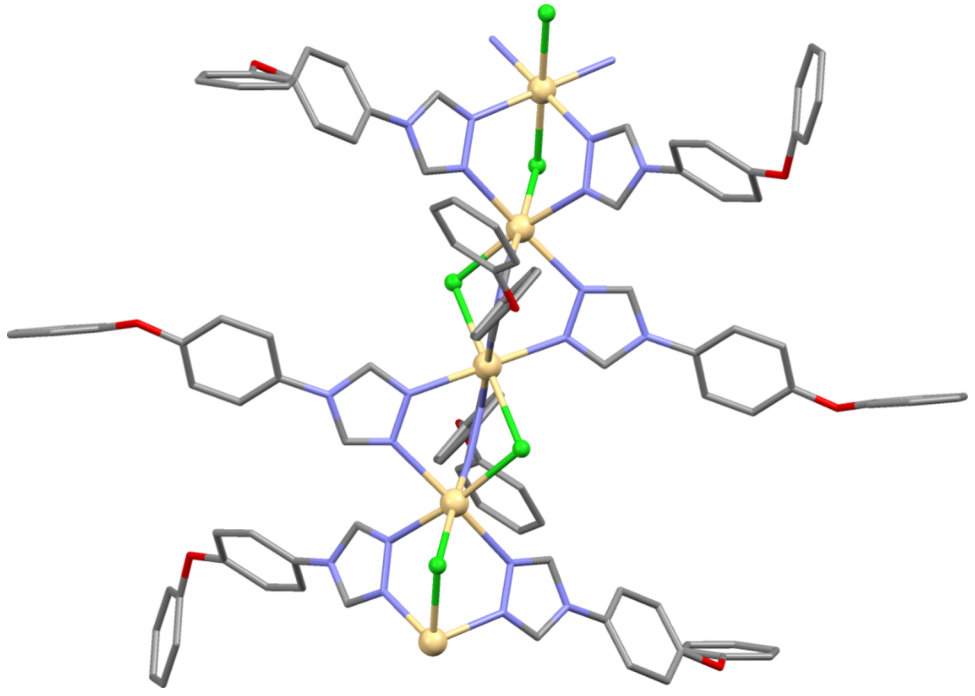

Figure 8. Extended stick representation of **6** showing the arrangement into a 1D chain, with ***ptt*** and chloride bridging Cd(II) ions.

tetrahedral coordination sphere around the Hg(II) cation, with a τ_4 value of 0.75.[37] As can be seen from Figure 7, complex **5** is highly isostructural with **4** at the molecular level, up to the relative orientation of the aromatic rings. As in **4**, the Hg(II) cation is four-coordinated by two N atoms from two different 1,2,4-triazole groups and two halogen atoms (Br).

In the crystal packing, $[HgBr_2(\textbf{\textit{ppt}})_2]$ units stack onto each other along the 2-fold axis, stabilized by parallel displaced $\pi-\pi$

DOI: 10.1021/acs.cgd.9b00734
Cryst. Growth Des. 2019, 19, 5292−5307

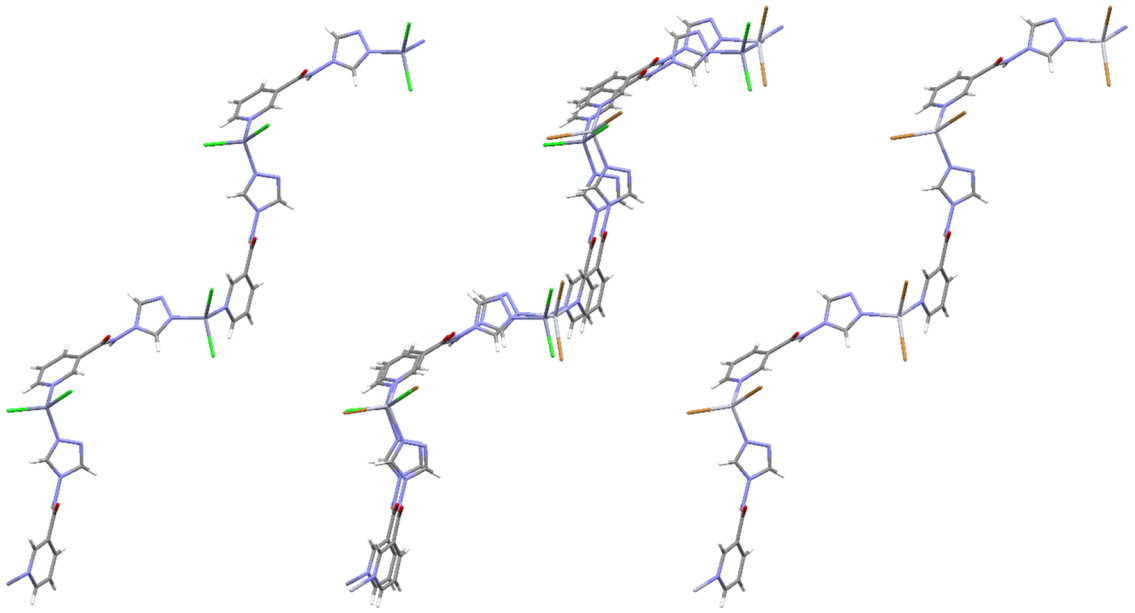

Figure 9. (left) 1D infinite chain generated by Zn(II) nodes and ***tpca*** linkers in **7**. (right) Isostructural $HgBr_2$ analogue in **8**. (middle) Superposition of **7** and **8**.

stacking between the 1,2,4-triazole ring and the central phenyl ring of the stacked unit. This interaction is characterized by a centroid−centroid distance of 3.802(5) Å, a dihedral angle α between the rings of 13.9(5)°, and a β angle of 16.2°. Slippage is calculated as 1.063 Å. Similar stacking patterns were also noticed in **4**; however, due to the orientation of the aromatic rings, classifying these interactions as $\pi-\pi$ stacking is less obvious.

*2.2.8. Crystal Structure of [Cd_2Cl_2(**ppt**)$_4$]($CdCl_4$)·4DMF (**6**).* Complex **6** crystallizes in the triclinic space group $P\bar{1}$ (Figure 8). The asymmetric unit contains a charged Cd complex consisting of three independent Cd(II) cations, two of which are located on inversion centers, two chloride atoms, and four ***ppt*** ligands. A negatively charged $[CdCl_4]^{2-}$ anion assures charge neutrality, and four lattice DMF molecules occupy the lattice voids. The $[Cd_2Cl_2(\textbf{ppt})_4]^{2+}$ cations form a 1D CP where each Cd(II) ion is surrounded by two chloride atoms and four nitrogen atoms belonging to four different ***ppt*** ligands, in a distorted-octahedral CdN_4Cl_2 geometry with distortion parameters Σ, θ,[41] for the central Cd(II) cation of 52, 359°, 21, 360°, and 29°, 360° for the Cd(II) ions located on the inversion centers. As such, consecutive Cd(II) cations are triply bridged by a single Cl atom and two *N*,*N*-triazole bridging ***ppt*** ligands, in a triangular arrangement, with a Cd···Cd distance of 3.798 and 3.813 Å.

*2.2.9. Crystal Structure of [$ZnCl_2$(**tpca**)] (**7**).* Compound **7** crystallizes in the monoclinic space group $P2_1/c$, and its asymmetric unit contains one formula unit. The Zn(II) ion is four-coordinated via two N atoms (one from the triazole ring and one from the pyridine ring) of the two bridging ***tpca*** ligands and two chloride atoms (Figure 9) to form a distorted-tetrahedral ZnN_2Cl_2 geometry with the distortion parameter τ_4 = 0.90.[37] The adjacent Zn(II) ions are linked by ***tpca*** ligands to form an infinite wavy chain with a Zn···Zn distance of 10.371 Å.

*2.2.10. Crystal Structure of [$HgBr_2$(**tpca**)] (**8**).* The CP chain formed between $HgBr_2$ and ***tpca*****8** is isostructural with **7** (Figure 9); the increase in unit cell volume from 1164 to 1300 Å^3 can be attributed to the larger volume occupied by the Hg and Br atoms, in comparison to the Zn(II) and Cl(II) ions. The distortion parameter τ_4 is 0.77.[37]

*2.2.11. Crystal Structure of [Cd(**tpca**)$_2$(H_2O)$_2$]·2H_2O (**9**).* CP **9** crystallizes in the monoclinic space group $C2/c$. The asymmetric unit contains a Cd(II) cation, one deprotonated ***tpca*** ligand, one coordinated water molecule, and one free lattice water molecule. As shown in Figure 10, the Cd(II) ion sits in a distorted-octahedral CdN_4O_2 geometry with the equatorial positions taken by four nitrogen atoms (two from the triazole ring and two from the pyridine ring) of the four bridging ***tpca*** ligands. Axial positions are filled by two coordinated water molecules.

The structure can be described as two interpenetrating 2D square-grid CPs (along the *bc* plane) with dimensions of 11.545 × 11.545 Å and diagonal-to-diagonal Cd···Cd distances of 16.096 × 16.556 Å. It is constructed from 36-membered nonplanar rings. Each ring is built from four Cd(II) centers bridged by four ***tpca*** ligands with coordination mode II (Scheme S2). The structure of **9** affords a 4-connected uninodal 2D network with point Schläfli symbol $\{4^4.6^2\}$ and exhibits a sql net topology.[38] The cavities are occupied by free lattice water molecules that in combination with the coordinated water molecules extend the 2D interpenetrating CPs into a 3D framework through hydrogen bonding (Figure 10).

2.3. Luminescent Properties. Emission and excitation spectra of compounds **1**−**9**, as well as those of the corresponding ligands (***btpm***, ***tpca***, and ***ppt***) were investigated at room temperature in the solid state (Figure 11). While all of the CPs were found to display a conspicuous blue to blue-green ligand-based luminescence, which is typically observed for many d^{10} metal complexes carrying N-donor aromatic subunits fixed in a favorable structural orientation,[42−44] the nature of the emissive excited states shows a remarkable diversity, as will be further discussed below.

The luminescence spectrum of the free ***btpm*** ligand consists of two bands with emission maxima at λ = 370 nm and λ = 485 nm, respectively (Figure 11). The short-wavelength component of the luminescence spectrum with a narrow bandwidth and a rather small Stokes shift can be tentatively assigned to the normal "locally excited" ligand-centered (LC) fluorescence involving the aromatic π-electron system,[45] while the additional

DOI: 10.1021/acs.cgd.9b00734
Cryst. Growth Des. 2019, 19, 5292−5307

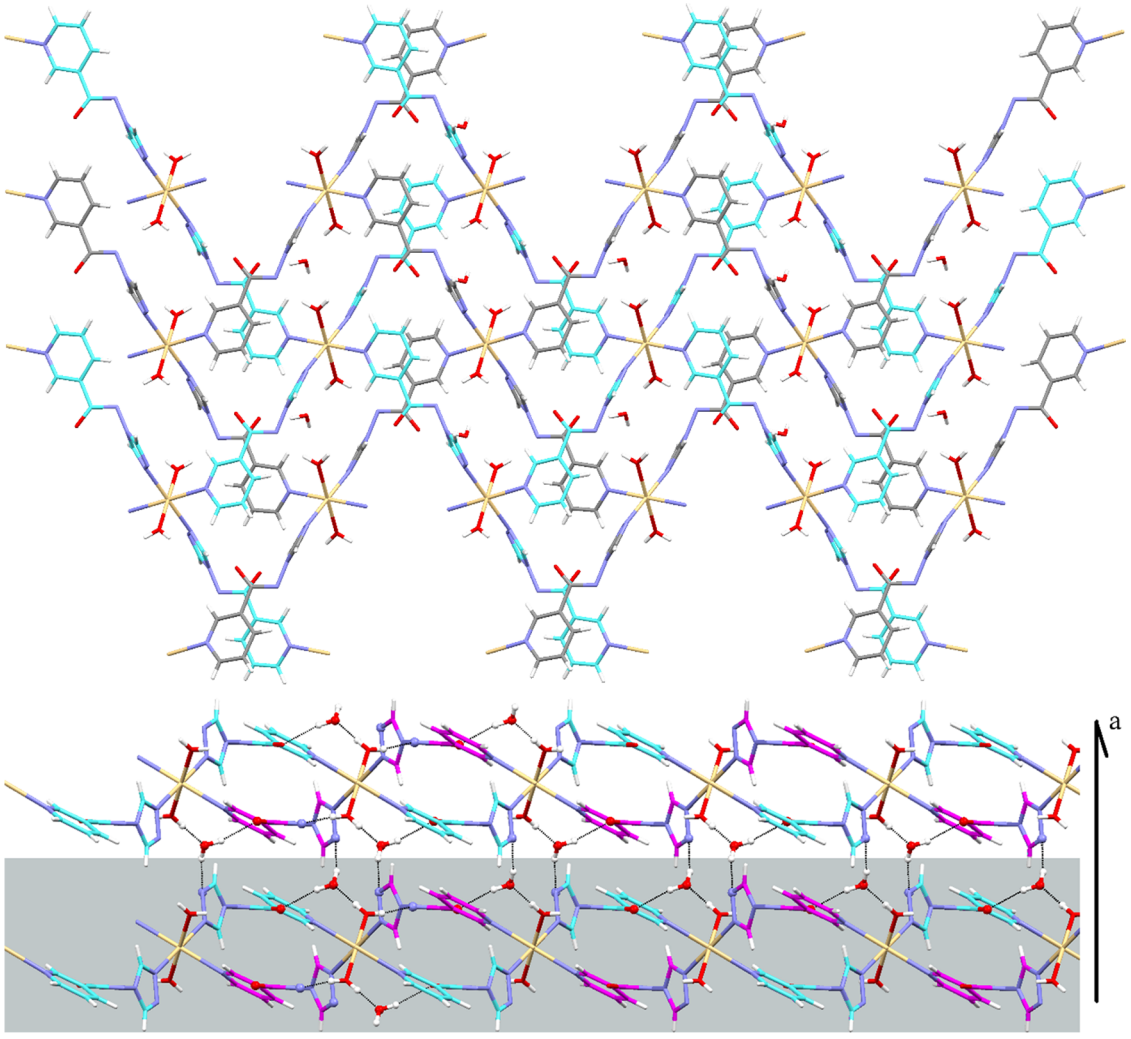

Figure 10. (top) Expanded model of **9** showing the two interpenetrating 2D networks formed by connecting octahedral Cd(II) cations through ***tpca*** ligands (the two networks are represented with either gray or cyan carbon atoms). (bottom) Hydrogen-bonding network involving the coordinated and lattice water molecules, interconnecting the interpenetrating CPs (gray or magenta carbon atoms) as well as the stacked layers along the *a* axis (white and gray background colors).

broad and red-shifted band is ascribed to an intraligand charge transfer (ILCT) state involving both the 1,2,4-triazole and the phenyl moieties of the ***btpm*** ligand. In the latter case, the two aromatic rings are expected to approach a coplanar conformation with substantial degree of electronic coupling, thus causing the observed bathochromic shift of the luminescence spectrum. Such intramolecular charge transfer interactions essentially depending on the orientation of the aromatic ring systems have already been well-described for *N*-phenylpyrrole derivatives and related chromophores.[46,47] As an effect of the metal coordination, in the Zn(II) and Cd(II) complexes **1**−**3** the characteristic broad ILCT-type luminescence of the coordinated ***btpm*** ligand is slightly blue shifted with the corresponding band maxima occurring at λ = 480 nm and λ = 470 nm, respectively (Figure 11). For the Cd(II) compound **3**, an additional short-wavelength feature occurs in the luminescence spectrum as a shoulder at around λ = 440 nm. This difference between Zn(II) and Cd(II) complexes of ***btpm***, together with the energetic position,[48] might indicate the presence of ligand-centered phosphorescence in **3** due to increased spin−orbit coupling mediated by the coordinated Cd(II) cation. More detailed studies including luminescence lifetime measurements, however, would be necessary in order to further corroborate this assumption.

A quite similar luminescence behavior which can also be ascribed to the presence of the *N*-phenyltriazole subunit is observed in the case of the ***ppt*** ligand, as shown in Figure 11. Upon UV light excitation (350−360 nm), the free ligand shows an ILCT emission band at λ = 440 nm, which is hypsochromically shifted to λ = 430 nm in the d^{10} metal complexes **4**−**6**.

For the ***tpca*** systems studied, because of the different ligand structure, there is no indication for an ILCT interaction between the 1,2,4-triazole and the pyridine subunits, which would require the possibility to form a π-conjugated coplanar orientation directly coupling both aromatic rings. The ***tcpa*** luminescence spectrum recorded in the solid state can thus be interpreted as a regular fluorescence of the free ligand with a maximum at λ = 410 nm arising from a localized π−π^* transition, similar to the solid-state luminescence properties of other blue-light emitters with an aromatic carboxamide moiety.[49] Excitation spectra for the λ = 410 nm peak maximum support this assignment to a localized LC state ,as shown in the case of complex **8** by the presence of a conspicuous vibronic pattern originating from the emissive aromatic moiety. When the pyridine and the triazole

DOI: 10.1021/acs.cgd.9b00734
Cryst. Growth Des. 2019, 19, 5292−5307

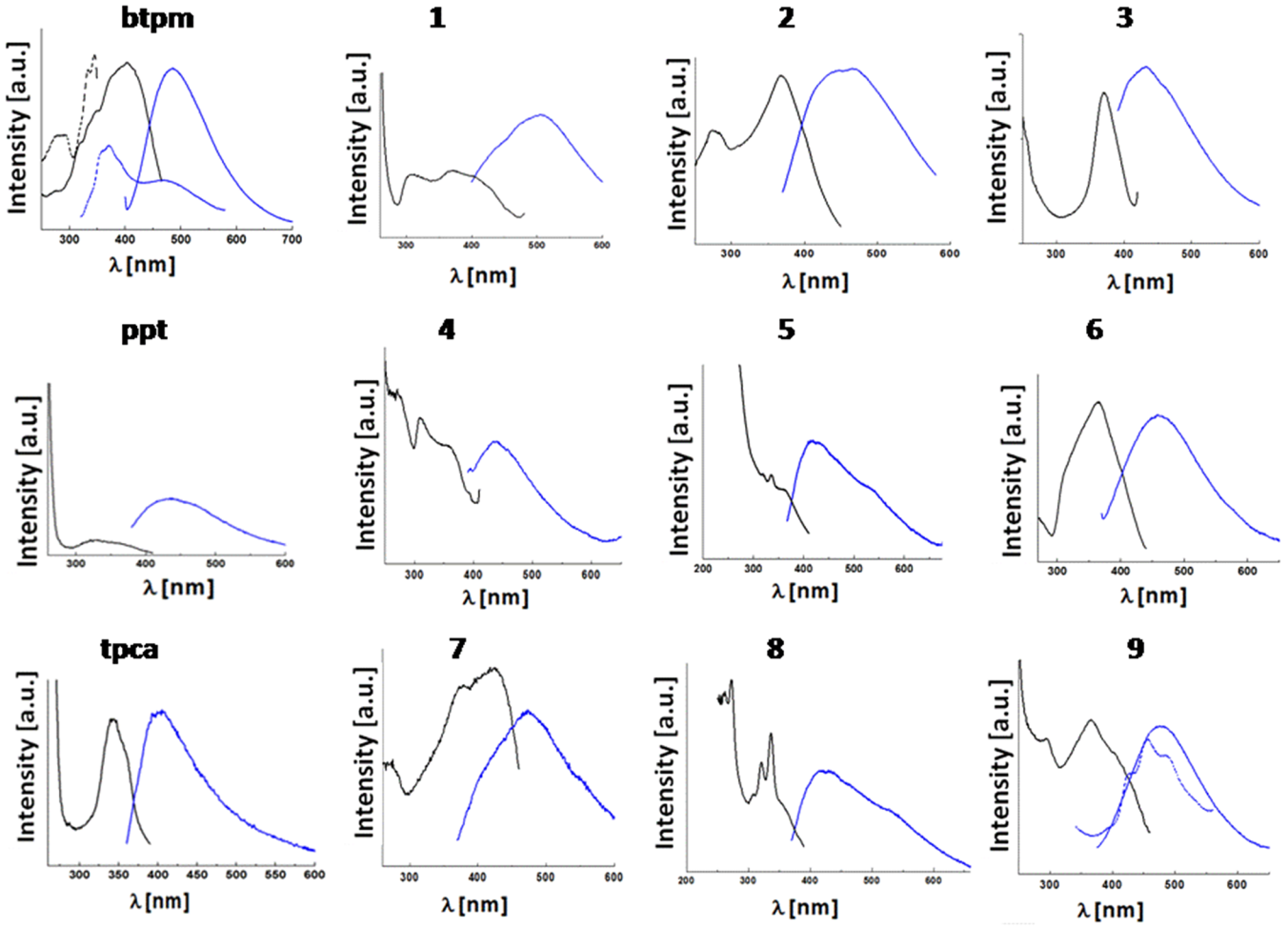

Figure 11. Luminescence and excitation spectra of ***btpm***, ***ppt***, ***tpca***, and **1**−**9** in the solid state at room temperature.

subchromophores of two different ***tcpa*** ligands, however, are arranged together by coordination to a common d^{10} metal center, the dominant part of the luminescence spectrum may significantly shift to longer wavelengths (Figure 11). This approximation of donor and acceptor subunits mediated by metal complex formation can obviously give rise to luminescent ligand to ligand charge transfer (LLCT) states.[50] For the Cd(II)- and Hg(II)-containing CPs **8** and **7**, the maximum of this LLCT emission is observed at λ = 440 nm, which is quite similar in energy to the charge transfer states observed for compounds **1**−**4** and **6** and closely matches the band maximum in d^{10} metal complexes with electronically coupled pyridyl-tetrazole ligands.[51] The Zn derivative **7**, which also displays such a ***tpca***-based LLCT band at λ = 440 nm, quite remarkably also shows an additional peak with a maximum at around λ = 500 nm as the most prominent emission band. This luminescence feature, which is absent in complex **9**, can be ascribed to the presence of chloride ligands in **7** and is tentatively assigned to a low-lying halide to ligand charge transfer (XLCT) state,[52] corresponding to an electronic transition between the chloride donor and the ***tpca*** acceptor subunits of the Zn(II) complex. Such a preliminary assignment could be further confirmed by changing the halide donors X from chloride to bromide and iodide, which should then lead to an increasing red shift of the corresponding XLCT luminescence maximum. Indeed, available data in the literature reported for similar d^{10} metal coordination polymers based on 1,2,4-triazole-containing ligands clearly follow such a trend in their emission properties.[53] Moreover, the emission spectra of the Hg(II) complexes **5** and **8**, both carrying bromide ligands, also display such longer-wavelength luminescence features at λ = 540−550 nm, which corroborates the tentative assignment as halide to ligand type (XLCT) luminescence.

2.4. Electrochemistry. The electrochemical (EC) method is regarded as a promising synthesis route to CPs/MOFs as thin films, powders, and single crystals.[54] In particular, the EC method is a valuable alternative to solvothermal techniques, which often lead to decomposition of the starting reagents, to synthesize MOFs more quickly and potentially in a continuous mode.[55,56] The method is based on the dissolution of a metal anode in a solution containing the ligand molecule. When appropriate parameters are selected, the process can result in compact CP layers on the electrode. Of immense interest are the 2D graphene-like MOFs due to their multifunctionalities (e.g., electrical conductivity and fast sensing applications).[57] For this purpose, we have focused in this work on the 2D network $[Zn(\textbf{\textit{btpm}})_2(H_2O)](BF_4)_2{\cdot}2\textbf{\textit{btpm}}{\cdot}8H_2O$ (**2**). Several exploratory experiments were run in order to verify the feasibility of the EC synthesis of this 2D network **2**.

Electrodeposition resulted in the formation of an amorphous layer on the Zn electrode and a precipitate in the electrolyte. XRPD of the Zn electrode only shows peaks of Zn (Figure 12a). Investigation by X-ray powder diffraction of the precipitate collected by filtration demonstrated the amorphous character of the precipitate (Figure 12b) in contrast to the crystalline

DOI: 10.1021/acs.cgd.9b00734
Cryst. Growth Des. 2019, 19, 5292−5307

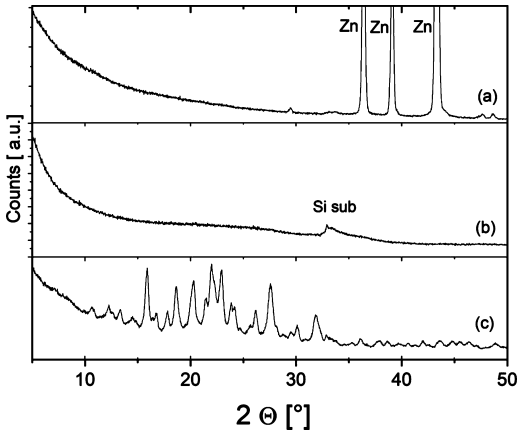

Figure 12. XRD patterns of **2** synthesized electrochemically as a layer (a) or as a powder (b) and as a microcrystalline powder from classic solution chemistry (c).

character of the microcrystalline powder obtained by classical solution chemistry (Figure 12c).

The SEM investigation of microcrystalline particles obtained by solution chemistry synthesis revealed crystallites of dodecahedral shape (Figure 13). This observation confirms

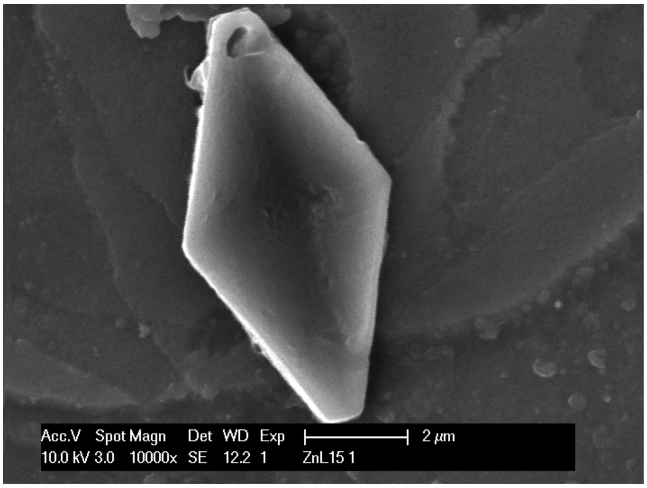

Figure 13. SEM picture of **2** synthesized from solution chemistry.

the crystalline character of **2** suggested earlier by XRD (Figure 12c) and confirmed by the obtainment of single crystals that were used to obtain the crystal structure of this material (Figure 4).

Figure 14 shows the SEM of powder samples synthesized electrochemically. The obtained agglomerates have dimensions similar to those synthesized by classic solution chemistry (Figure 13). However, spherical clusters with micrometric dimensions were identified. Magnification shows hollow structures of ~1 μm diameter with potential porous properties (Figure 14).

Electrochemically deposited layers of **2** consist of the same, well-intergrown particles as shown in Figure 14, but the coatings are often cracked (Figure 15) and do not show a crystalline XRD pattern (Figure 12a).

3. DISCUSSION

The CP architecture is governed not only by the length of the ligand spacer but also by the possible coordination number and modes of these modules connecting the metal centers. Moreover, the synthetic pathway also determines the topology outcome and the thereby associated properties. Using the versatile 1,2,4-triazole moiety as a building block, three flexible, bent ligands were synthesized: ***btpm***, a symmetric molecule, which can coordinate up to four metal centers and is prone to give potentially 1D, 2D, and 3D coordination polymers, ***tpca***, which is likely to act as a bridging ligand through the 1,2,4-triazole unit and the pyridine nitrogen, and ***ppt***, for which only the 1,2,4-triazole unit can coordinate, thereby leading at best to 1D coordination polymers (Scheme S1). Schemes S1−S3 give the possible coordination modes for these three molecules. The choice of flexible ligands over rigid ones allows more variety in the target structure, especially in combination with the bent character of the synthesized ligands. The influence of the anion was also investigated, limiting the coordination centers to group 12 transition metals.[58]

Recrystallization from water of the precipitate obtained by the self-assembly of the symmetrical V-shaped ***btpm*** molecule with $ZnCl_2$ by slow diffusion afforded the linear 1D coordination polymer $[ZnCl_2(\textbf{\textit{btpm}})]$ (**1**) by repetition of $ZnCl_2(\textbf{\textit{btpm}})$ units, with the ***btpm*** ligand acting as a bidentate bridging spacer (coordination mode III, Scheme S1) coordinating two tetrahedral Zn nodes, spaced out by 15.18(2) Å.

The anion plays a significant role in controlling the topology as well, since replacing Cl by with the weakly coordinating anion BF_4 resulted in the 2D coordination polymer $[Zn(\textbf{\textit{btpm}})_2(H_2O)](BF_4)_2{\cdot}2\textbf{\textit{btpm}}{\cdot}8H_2O$ (**2**). The ***btpm*** ligand coordinates as in **1**, but four ligands are arranged around every Zn(II) cation, and a coordinated water molecule completes the coordination sphere. Given that a crystallographic 2-fold symmetry axis coincides with the $Zn{-}O_w$ axis, the complex could be described as a distorted square pyramid, where the coordinated water molecule occupies the axial position. The distortion parameter τ_5 of 0.69, however, indicates a trigonal-pyramidal geometry.[59] Wang and co-workers[60] obtained under hydrothermal conditions the CP $[Zn_2(\textbf{\textit{btpm}})_3(H_2O)_4](NO_3)_4{\cdot}H_2O$, whose crystal structure shows interpenetrating sheets when ***btpm*** is reacted with $Zn(NO_3)_2$, showing the influence of the synthesis conditions on the overall topology. The reported structure has octahedral Zn geometries, and coordination modes I and III (Scheme S1) are both present. The hydrothermal reaction of ***btpm*** and $Cd(NO_3)_2$ provided $[Cd_2(\textbf{\textit{btpm}})_3(H_2O)_4](NO_3)_4{\cdot}3.5H_2O$ with a similar molecular structure.[60]

The use of strongly coordinating anions ($CdCl_2$) resulted in the compound $[Cd_3Cl_6(\textbf{\textit{btpm}})_2]{\cdot}8H_2O$ (**3**) under solvothermal conditions, which only shows the μ_4-tetradentate coordination mode (I in Scheme S1), and a bridging Cl anion takes the role of the ***btpm*** ligand. **3** forms a polymeric 1D chain by repetition of linear trinuclear Cd units; the central Cd(II) ion is positioned on an inversion center and on either side is coordinated by two bridging triazole moieties and a bridging Cl atom, adopting a distorted octahedron, with distortion parameters[41] $\Sigma = 56°$ and $\theta = 360°$. The terminal Cd(II) ions are also found in octahedral environments which are completed by three Cl atoms; two of these are bridging with a neighboring trinuclear unit, and one is a terminal Cl atom (distortion parameter $\Sigma = 85°$ and $\theta = 362°$). While octahedral geometries for Cd(II) are quite common, it is mostly observed with chelating ligands.

Although complexes $[ZnCl_2(\textbf{\textit{ppt}})_2]$ (**4**) and $[HgBr_2(\textbf{\textit{ppt}})_2]$ (**5**) are obtained by different reaction pathways, hydrothermal and slow diffusion, respectively, the overall conformations of

DOI: 10.1021/acs.cgd.9b00734
Cryst. Growth Des. 2019, 19, 5292−5307

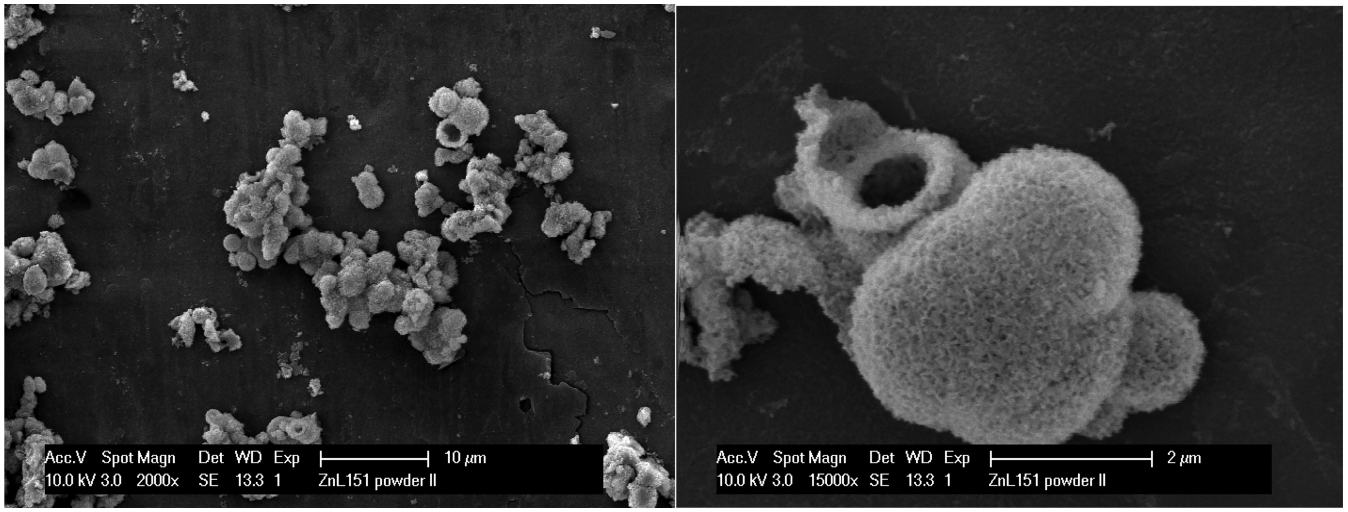

Figure 14. SEM pictures of a powder of **2** synthesized electrochemically at two magnifications showing a hollow structure.

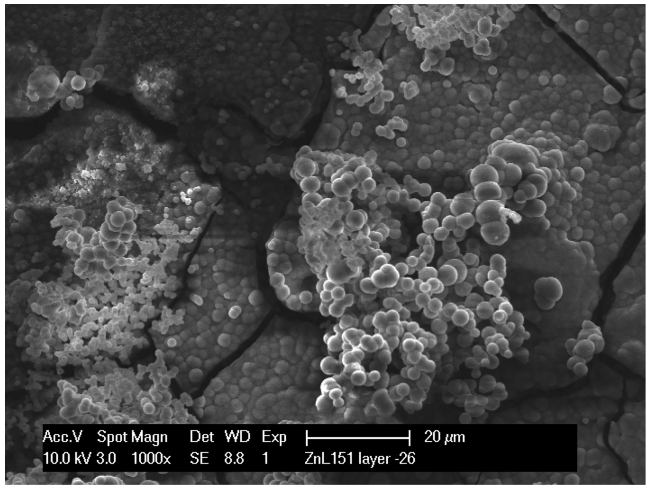

Figure 15. SEM pictures of several layers of **2** synthesized electrochemically on the Zn electrode.

these mononuclear complexes are very similar. A bivalent cationic 1D CP was observed in $[Cd_2Cl_2(\textbf{\textit{ppt}})_4]CdCl_4{\cdot}4DMF$ (**6**), where the weakly coordinating anion $CdCl_4^{2-}$ was surprisingly formed in situ. The ***ppt*** ligand is bridging two Cd(II) ions in coordination mode 1 (Scheme S3). **6** shows that coordinating anions can lead to unpredictable topologies, especially if the anions can behave as bridging entities, as they do here.

The situation with the ***tpca*** ligand is rather different. Indeed, in addition to coordination sites on either side of the ligand (triazole and pyridine), hydrogen bond donor (NH) and acceptor sites (C═O) are also present at the center of the ligand, with the potential of stabilizing the crystal structure. The reaction under solvothermal (DMF) conditions between $ZnCl_2$ and ***tpca*** provides the 1D coordination polymer $[ZnCl_2(\textbf{\textit{tpca}})]$ (**7**) in coordination mode II (Scheme S2), and the strongly coordinating Cl anions fill up the remaining sites in the tetragonal Zn environment (distortion parameter τ_4 = 0.93), hence limiting the coordination polymer beyond 1D. The coordination chain is built up from $ZnCl_2(\textbf{\textit{tpca}})$ units in a zigzag repetition. As expected, the N−H group hydrogen bonds to a terminal Cl atom from a neighboring 1D chain. The reaction of $HgBr_2$ and ***tpca*** yields the isostructural 1D chain $[HgBr_2(\textbf{\textit{tpca}})]$ (**8**), with identical hydrogen-bonding interactions. The reaction of $CdSO_4$ with ***tpca*** under similar conditions yields $[Cd(\textbf{\textit{tpca}})_2(H_2O)_2]{\cdot}2H_2O$ (**9**), a 2D CP also with the ***tpca*** ligands in coordination mode II (Scheme S2). Four ***tpca*** ligands are coordinated around a single Cd metal center (positioned on an inversion center) on the equatorial sites of an octahedron (distortion parameters Σ = 15°; θ = 360°). Opposite ***tpca*** ligands are coordinated through either the 1,2,4-triazole or pyridine moiety, with two coordinated water molecules topping the axial positions of the octahedron. Surprisingly, the anions are not present in the crystal structure and the ***tpca*** ligand is negatively charged, resulting in a deprotonated NH group and a lengthening of the C−O bond (single-bond character) as well as the observed double-bond character of the amide bond. More extended hydrogen bonding is present through the central hydrogen bonding sites, and both sites interact with either isolated or coordinated water molecules. The former is involved in three hydrogen bonds (Table S10) and glues together two ***tpca*** ligands through the C═O and 1,2,4-triazole units and a coordinated water molecule.

4. CONCLUSION

In this paper, we have presented the structural investigation of a series of seven Zn(II)/Cd(II)/Hg(II) coordination polymers exhibiting various types of molecular architectures as well as two mononuclear complexes made of 1,2,4-triazole building blocks. The construction of these coordination polymers demonstrates that the substituents on the 1,2,4-triazole ring and the anions are critical in determining the molecular architecture and topologies of the metal-triazole coordination polymers. All of the complexes exhibit intense blue luminescence of different origin in the solid state at room temperature (including examples of dual emission), which have been tentatively assigned to involve low-lying excited states giving rise to electronic transitions of ligand-centered or charge transfer type. Electrochemical synthesis of the 2D network **2** was successfully carried out, revealing hollow particles.

5. EXPERIMENTAL SECTION

5.1. Materials and Physical Measurements. *5.1.1. Chemicals.* $CdCl_2$, $CdSO_4$, $SOCl_2$, $NH_2{-}NH_2{\cdot}H_2O$, and nicotinic hydrazide ($C_6H_7N_3O$) were provided by Acros Organics. $ZnCl_2$ was provided by Sigma-Aldrich, whereas $Zn(BF_4)_2{\cdot}H_2O$ was provided by Strem

DOI: 10.1021/acs.cgd.9b00734
Cryst. Growth Des. 2019, 19, 5292−5307

Chemicals. 4,4′-Methylenedianiline and 4-phenoxyaniline were purchased from TCI Chemicals. All other chemicals were standard reagent grade and were sed as supplied. *N*,*N*-Dimethylformamide azine dihydrochloride and bis(4-(1,2,4-triazol-4-yl)phenyl)methane (***btpm***) were prepared according to our literature procedure.[33]

5.1.2. Physical Measurements. Elemental analyses for C, H, and N were performed on a Thermo FinniganFlashEA 1112 CHNS-O Analyzer as well as an instrument by MEDAC, UK. Mass spectra were recorded in methanol on a Thermo Finnigan LCQ Ion Trap spectrometer in ESI mode, detecting positive ions. ^{1}H NMR spectra were recorded in DMSO-d_6 solution with tetramethylsilane (TMS) as an internal standard at ambient temperature on a Bruker AC 300 MHz spectrometer. FT-IR spectra were recorded as KBr pellets on a Shimadzu IRAffinity-1 FT-IR spectrophotometer (50 scans with a resolution of 4 cm^{-1} in the range 400−4000 cm^{-1}). The luminescence measurements were carried out in the solid state at room temperature using a Horiba JobinYvon Fluorolog-3 spectrofluorometer equipped with two double-grating monochromators, a R928P photomultiplier, and an FL-1040 phosphorimeter. All emission spectra were corrected for wavelength-dependent instrument and detector response and verified by collecting the corresponding excitation spectra. All electrochemical experiments were controlled with an EG&G potentiostat/galvanostat (Model 273). A small electrochemical cell (10 mL) including a Pt foil (ca. 5 cm^2) as the counter electrode, a homemade Ag/AgCl (3 M KCl) electrode as the reference, and a zinc anode was used. All plates (ca. 0.5 cm^2) were polished and cleaned with ethanol before being used in the cell. The electrolyte was based on the same concentration as that for the ***btpm*** molecule used for the solution synthesis of **2** (53 mg/25 mL, or 21 g/L) with 4.8 g/L of $NaBF_4$ to compensate for the absence of BF_4^- ions normally introduced in the solution with the metal salt. To compensate for the absence of water molecules in the bath normally supplied by the metal salt, a methanol/water mixture (9/1) was used as solvent. X-ray powder diffraction experiments were carried out on a Bruker AXS D8 diffractometer using Cu Kα radiation (λ = 0.15405 nm) and Ni filter with 2θ ranging from 5 to 80° with a step size of 0.02° (1.0 s per step) at 40 kV. Scanning electron microscopy was performed on a FEI Nova NanoSEM 450 instrument.

5.2. Synthesis and Characterization. *5.2.1. 1-(4-Phenoxyphenyl)-1,3,4-triazole (**ppt**).* In a solution of 4-phenoxyaniline (1 g, 5.4 mmol, 1 equiv) in 20 mL of toluene was suspended *N*,*N*-dimethylformamide azine dihydrochloride (1 g, 9 mmol, 1 equiv). The slurry was heated to 80 °C for 2−24 h until complete dissolution was reached. The progress of the reaction was monitored by TLC. The reaction mixture was first cooled to room temperature and then to 5 °C. The resulting precipitate was washed with 2 mL of cold ethanol and 5 mL of Et_2O, and dried in air. Recrystallization from MeOH afforded colorless single crystals. Yield: 0.53 g (42%). Mp: 180 °C. MS-ESI (*m*/*z*): 238 [M + H]$^+$. Anal. Calcd for $C_{14}H_{11}N_3O$·2.5EtOH: C, 64.75; H, 7.44; N, 11.92. Found: C, 64.95; H, 4.64; N, 11.63. ^{1}H NMR (300 MHz, DMSO-d_6): δ 9.08 (s, 2H, CH of trz), 7.70 (m, 2H, ph), 7.20 (m, 2H, ph), 7.17 (m, 2H, ph), 7.09 (m, 3H, ph), 7.06 (m, 1H, ph) ppm. FT-IR (KBr at room temperature): ν 3423 (s), 3112 (s), 1683 (m), 1585 (s), 1510 (s), 1311 (w), 1284 (m), 1078 (s), 1020 (s), 946 (w), 649 (s), 623 (m), 530 (s), 449 (m) cm^{-1}.

*5.2.2. N-(1,2,4-Triazol-4-yl)pyridine-3-carboxamide (**tpca**).* A mixture of azine (3.13 g, 14.55 mmol, 1 equiv) and nicotinic hydrazide (1 g, 7.28 mmol, 1 equiv) was refluxed with vigorous stirring for 24 h in toluene (20 mL). The white precipitate obtained was collected by filtration, washed with ethanol and Et_2O, and dried in air. Recrystallization from MeOH gave colorless crystals. Yield: 0.73 g (51%). Mp: 120 °C. MS-ESI (*m*/*z*): 190 [M + H]$^+$. Anal. Calcd for ***tpca***·H_2O: C, 46.60; H, 3.91; N, 33.97. Found: C, 45.14; H, 3.88; N, 33.85.^{1}H NMR (300 MHz, DMSO-d_6): δ 12.63 (br, s,1H, NH), 9.16 (d, 1H, py), 8.80 (s, 2H, CH, trz), 8.38 (d, 1H, py),7.66 (dd, 2H, py). FT-IR (KBr at room temperature): ν 3339(w), 3127 (s), 3053 (s), 3022 (s), 2974 (s), 2837 (s), 2779 (s), 2440 (m), 1682 (vs), 1589 (vs), 1420 (s), 1402 (s), 1325 (s), 1281 (vs), 1238 (m), 1202 (vs), 1134 (m), 1099 (s), 1069 (vs), 1020 (s), 964 (s), 943 (s), 903 (s), 829 (s), 708 (vs), 673 (s), 615 (vs), 446 (s), 420 (w) cm^{-1}.

*5.2.3. [$ZnCl_2$(**btpm**)] (**1**).* To a stirred hot solution of 10 mL of ***btpm*** (0.44 g, 2 equiv) in methanol was added dropwise $ZnCl_2$ (0.1 g, 1 equiv in 2 mL of methanol). The mixture was stirred overnight at room temperature. The precipitated yellowish white solid was filtered, washed with MeOH and Et_2O, and dried under vacuum. Recrystallization from a hot MeOH/H_2O solution (3/7 v/v) afforded needle-shaped single crystals, suitable for X-ray analyses. Yield: 0.28 g (68%). Anal. Calcd for [$ZnCl_2(C_{17}H_{14}N_6)$]: C, 46.55; H, 3.22; N, 19.16. Found: C, 46.22; H, 3.17; N, 18.83. FT-IR (KBr at room temperature): ν 3117 (m), 3100 (s), 3051 (m), 2986 (m), 1537 (vs), 1464 (m), 1429 (s), 1369 (w), 1339 (w), 1314 (m), 1279 (s), 1248 (s), 1227 (s), 1123 (w), 1097 (vs), 1043 (vs), 1018 (s), 982 (m), 968 (m), 868 (s), 702 (w), 667 (m), 640 (s), 534 (s), 424 (w) cm^{-1}.

*5.2.4. [Zn(**btpm**)$_2$(H_2O)](BF_4)$_2$·2btpm·8H_2O (**2**).* A procedure similar to that for **1** was used with $Zn(BF_4)_2$·H_2O (0.20 g, 1 equiv) and ***btpm*** (0.76 g, 3 equiv), affording needle-shaped single crystals. Yield: 0.46 g (16%). Anal. Calcd for [$Zn(C_{17}H_{14}N_6)_2(H_2O)$]($BF_4$)$_2$·2$C_{17}H_{14}N_6$·5$H_2O$: C, 52.44; H, 4.40; N, 21.60. Found: C, 52.64; H, 3.97; N, 21.79. FT-IR (KBr at room temperature): ν 3049 (m), 3202 (w), 3100 (s), 2909 (w), 1908 (w), 1680 (m), 1653 (w), 1608 (m), 1589 (w), 1525 (vs), 1427 (m), 1366 (m), 1337 (m), 1312 (m), 1242 (vs), 1200 (m), 1098 (vs), 1061 (vs), 984 (m), 918 (m), 818 (s), 793 (s), 662 (m), 638 (s), 532 (s), 455 (w) cm^{-1}.

*5.2.5. [Cd_3Cl_6(**btpm**)$_2$]·8H_2O (**3**).* $CdCl_2$(18.9 mg, 0.08 mmol, 1 equiv) and ***btpm*** (50 mg, 0.16 mmol, 2 equiv) were dissolved in DMF (6 mL). The reaction mixture was stirred for 0.5 h at room temperature, moved to a 25 mL Teflon reactor, heated to 120 °C for 3 days, and cooled at room temperature. Colorless crystals suitable for single-crystal X-ray studies were obtained after 10 days of slow evaporation. Yield: 26 mg (22%). Anal. Calcd for [$Cd_3Cl_6(C_{17}H_{14}N_6)_2$]·10$H_2O$: C, 30.58; H, 3.63; N, 12.59. Found: C, 30.12; H, 4.60; N, 13.38. FT-IR (KBr at room temperature): ν 3096 (m), 1699 (w), 1649 (w), 1537 (vs), 1396 (w), 1364 (w), 1339 (w), 1313 (w), 1304 (w), 1250 (m), 1128 (w), 1098 (m), 1016 (m), 982 (w), 868 (m), 822 (m), 640 (m), 567 (w), 530 (m), 420 (w) cm^{-1}.

*5.2.6. [$ZnCl_2$(**ppt**)$_2$] (**4**).* A procedure similar to that for **3** was used with $ZnCl_2$ (13.63 mg, 0.1 mmol, 1 equiv) and ***ppt*** (50 mg, 0.21 mmol, 2 equiv). Colorless crystals suitable for single-crystal X-ray studies were obtained after 1 week of slow evaporation. Yield: 22 mg (13%). Anal. Calcd for [$ZnCl_2(C_{14}H_{11}N_3O)_2$]: C, 55.06; H, 3.63; N, 13.76. Found: C, 54.24; H, 3.27; N, 11.48. FT-IR (KBr at room temperature): ν 3105 (m), 3065 (m), 3009 (m), 2882 (w), 1543 (vs), 1510 (s), 1487 (s), 1325 (m), 3152 (w), 1244 (vs), 1171 (m), 1071 (m), 1017 (m), 982 (m), 899 (m), 872 (m), 845 (s), 756 (s), 691 (m), 644 (m), 594 (w), 517 (m), 488 (w) cm^{-1}.

*5.2.7. [$HgBr_2$(**ppt**)$_2$] (**5**).* A solution of ***ppt*** (50 mg, 0.21 mmol, 1 equiv) in MeOH (10 mL) was added dropwise to a solution of $HgBr_2$ (75 mg, 0.20 mmol, 1 equiv) in MeOH (5 mL). The clear solution was allowed to stand for 2 weeks at room temperature, after which colorless pillar crystals were filtered off, washed with MeOH, and dried in air. Yield: 70 mg (29%). Anal. Calcd for $C_{28}H_{22}Br_2HgN_6O_2$: C, 40.28; H, 2.66; N, 10.07. Found: C, 40.37; H 2.59; N, 10.01. FT-IR (KBr at room temperature): ν 3053 (m), 2914 (w), 2830 (m), 1618 (m), 1433 (w), 1310 (s), 1251 (m), 1001 (m), 768 (s), 699 (m), 638 (s) cm^{-1}.

*5.2.8. [Cd_2Cl_2(**ppt**)$_4$]($CdCl_4$)·4DMF (**6**).* A procedure similar to that for **3** was used with $CdCl_2$ (24 mg, 0.11 mmol, 1 equiv) and ***tpca*** (50 mg, 0.21 mmol, 2 equiv). Colorless crystals suitable for single-crystal X-ray studies were obtained after 8 weeks of slow evaporation. Yield: 15 mg (14%). Anal. Calcd for [$Cd_2Cl_2(C_{56}H_{44}N_{12}O_4)$]($CdCl_4$)$_3$·DMF: C, 34.06; H, 2.47; N, 8.75. Found: C, 34.98; H, 2.36; N, 8.34. FT-IR (KBr at room temperature): ν 3267 (w), 3190 (w), 3152 (w), 3111 (m), 2943 (w), 2886 (w), 1657 (w), 1589 (s), 1535 (vs), 1487 (vs), 1456 (s), 1433 (m), 1327 (w), 1277 (s), 1200 (s), 1163 (s), 1096 (s), 1074 (m), 984 (m), 941 (w), 841 (vs), 692 (s), 660 (m), 594 (w), 527 (s), 432 (w), 421 (w) cm^{-1}.

*5.2.9. [$ZnCl_2$(**tpca**)] (**7**).* $ZnCl_2$ (18 mg, 0.13 mmol, 1 equiv) and ***tpca*** (50 mg, 0.26 mmol, 2 equiv) were dissolved in water (8 mL). The reaction mixture was stirred for 0.5 h at room temperature, moved to a 25 mL Teflon reactor, heated to 120 °C for 3 days, and cooled to room temperature. Colorless crystals suitable for single-crystal X-ray studies

DOI: 10.1021/acs.cgd.9b00734
Cryst. Growth Des. 2019, 19, 5292−5307

were obtained after 2 weeks of slow evaporation. Yield: 25 mg (58%). Anal. Calcd for $[ZnCl_2(C_8H_7N_5O)]\cdot H_2O$: C, 27.96; H, 2.64; N, 20.39. Found: C, 27.09; H, 2.21; N, 19.34. FT-IR (ATR at room temperature): ν 3146 (m), 3125 (m), 3084 (w), 3001 (w), 2976 (w), 2793 (w), 1647 (w), 1611 (s), 1545 (m), 1530 (m), 1506 (s), 1476 (s), 1410 (m), 1292 (s), 1200 (w), 1113 (m), 1101 (w), 1070 (s), 1055 (m), 1020 (m), 953 (m), 937 (w), 876 (m), 829 (w), 785 (w), 739 (m), 694 (m), 675 (m), 621 (m), 525 (w), 436 (m), 417 (w) cm^{-1}.

*5.2.10. [$HgBr_2$(**tpca**)] (**8**).* A procedure similar to that for **5** was used with $HgBr_2$ (95 mg, 0.26 mmol, 1 equiv) and ***tpca*** (50 mg, 0.26 mmol, 1 equiv). Colorless crystals suitable for single-crystal X-ray studies were obtained after 1 week after slow evaporation. Yield: 60 mg (35%). Anal. Calcd for $[HgBr_2(C_8H_7N_5O)]\cdot 0.5MeOH$: C, 18.05; H, 1.6; N, 12.38. Found: C, 18.53; H, 1.41; N, 13.34. FT-IR (KBr at room temperature): ν 3134 (vs), 2940 (m), 1644 (s), 1500 (m), 1435 (m), 1300 (m), 1211 (w), 1091 (m), 920 (m), 775 (w), 670 (w), 645 (w) cm^{-1}.

*5.2.11. [Cd(**tpca**)$_2$(H_2O)$_2$]·2H_2O (**9**).* A procedure similar to that of **6** was used with $CdSO_4\cdot H_2O$ (34 mg, 0.13 mmol, 1 equiv) and ***tpca*** (50 mg, 0.26 mmol, 2 equiv). Colorless crystals suitable for single-crystal X-ray studies were obtained after 1 week of slow evaporation. Yield: 30 mg (34%). Anal. Calcd for $[Cd(C_8H_7N_5O)_2(H_2O)_2]\cdot 4H_2O$: C, 32.18; H, 4.05; N, 23.47. Found: C, 32.11; H, 3.12; N, 22.91. FT-IR (KBr at room temperature): ν 3206 (s), 3129 (s), 3158 (s), 1715 (m), 1649 (s), 1587 (s), 1560 (vs), 1528 (s), 1447 (m), 1337 (s), 1258 (w), 1198 (m), 1140 (m), 1107 (w), 1034 (m), 1013 (m), 963 (w), 936 (m), 835 (w), 806 (w), 743 (m), 665 (m), 631 (m), 557 (w), 503 (m), 465 (m) cm^{-1}.

5.3. Single-Crystal X-ray Diffraction. Single-crystal X-ray diffraction data of **1**−**9** and ***tpca*** were collected on a MAR345 image plate detector using Mo Kα radiation (λ = 0.71073 Å) either at ambient temperature or flash cooled to 150 K in a gaseous N_2 flow. The data were integrated with the CrysAlis^{Pro}software.[61] The implemented empirical absorption correction was applied. The structures were solved by direct methods using the SHELXT program[62] and refined by full-matrix least squares on $|F^2|$ using SHELXL2014/7.[62] Non-hydrogen atoms were anisotropically refined, and the hydrogen atoms were placed on calculated positions in riding mode with temperature factors fixed at 1.2 times U_{eq} of the parent atoms and 1.5 times U_{eq} for methyl groups. Figures were generated using Mercury software.[63] Crystallographic data are given in Table 1.

The crystal of ***tpca*** was found to be twinned (two domains); the twin matrix was determined by the TWINROTMAT procedure in Platon, and the final stages of refinement were done against HKLF5 formatted data. Several crystals of **1** were tested but showed rather poor diffraction quality. As such, a data cutoff of 1A was imposed during data reduction, beyond which the crystal diffracted poorly, even with a low-temperature (150 K) data collection. The measured crystals were found to be twinned, and refinement was done against a multi-hklf4, with reflections from both twin domains scaled to the twin fractions. Overall, data reduction statistics are rather poor as can be seen in Table 1. **2** contains several isolated lattice water molecules, for which not all hydrogen atoms could be located. This is due to the high degree of freedom which is available to these water molecules, due to the large pore size they reside in. For the water molecules where the hydrogen atoms could be localized in the density maps, the complete water molecule was refined as an idealized rigid group or the hydrogens were refined as riding on the parent O atom. Furthermore, the BF_4^- anion is disordered over two sites, illustrating the mobility of the molecules inside the large cavities. The use of isotropic restraints and enhanced rigid bond restraints was necessary to correctly refine the disordered anion. **3** also contains a large void filled with isolated water molecules. No hydrogens could be localized in the density maps, and the hydrogen bonding patterns could not be rationalized. The remaining void volume was treated with the Platon squeeze algorithm (204 Å^3).[40] Whole-molecule disorder (about 6% for the minor fraction) was detected but was only visible for the heavy-atom cluster (Cd and Cl atoms). The disordered $[ZnCl_2(\textbf{\textit{ppt}})_2]$ complex found on the 2-fold axis in the crystal structure of **4** was refined with an overall rigid bond restraint. The terminal phenyl group in **5** showed signs of movement in the form of elongated thermal ellipsoids and were subjected to a rigid bond restraint. **6** was integrated as a nonmerohedral twin and refined against a HKLF5 formatted reflection file. Due to the geometric constraints of the diffractometer (single ψ axis), in combination with the observed twinning, only 96.5% data completeness was reached. **6** contains three DMF solvent molecules, one of which was found disordered over two sites. Some restraints on the thermal ellipsoids were necessary to allow the refinement to converge, especially for the solvent molecules, for which isotropic and rigid bond restraints were applied, and thermal ellipsoids of the minor fraction of the disordered DMF molecule were constrained to be identical with the major part (72/28 ratio). Some large residual density peaks close to the Hg metal center are present in **8**, which are probably due to a combination of absorption and truncation errors during the Fourier transform. In **9** the lattice water molecule was idealized and refined as a rigid group able to rotate around the central O atom.

A suitable crystal of ***ppt*** was selected and mounted on a nylon loop on a SuperNova Dual Cu at zero diffractometer, equipped with an Atlas CCD detector. The crystal was kept at 100 K during data collection. Using Olex2,[64] the structure was solved with ShelXS,[65] the structure solution program using direct methods and refined with ShelXL,[62] and the refinement package using least-squares minimization. Non-hydrogen atoms were anisotropically refined and hydrogen atoms were placed in the riding mode with isotropic temperature factors fixed at 1.2 times U_{eq} of the parent atoms. CCDC 1918038−1918047 and 1920056 (***ppt***) contain supplementary crystallographic data for this paper. These data can be obtained free of charge from The Cambridge Crystallographic Data Centre via www.ccdc.cam.ac.uk/structures

■ ASSOCIATED CONTENT

Supporting Information

The Supporting Information is available free of charge on the ACS Publications website at DOI: 10.1021/acs.cgd.9b00734.

Overview of IR, TGA and crystallographic data (PDF)

Accession Codes

CCDC 1918038−1918047 and 1920056 contain the supplementary crystallographic data for this paper. These data can be obtained free of charge via www.ccdc.cam.ac.uk/data_request/cif, or by emailing data_request@ccdc.cam.ac.uk, or by contacting The Cambridge Crystallographic Data Centre, 12 Union Road, Cambridge CB2 1EZ, UK; fax: +44 1223 336033.

■ AUTHOR INFORMATION

Corresponding Author

*E-mail for Y.G.: yann.garcia@uclouvain.be.

ORCID

Kristof Van Hecke: 0000-0002-2455-8856

Yann Garcia: 0000-0002-3105-0735

Notes

The authors declare no competing financial interest.

■ ACKNOWLEDGMENTS

We acknowledge financial support from the FNRS (PDR T.0102.15, CDR 33694457), Walloon region (MEMLINK), WBI for a stipendium of excellence for H.B. and the Foundation for Polish Science for financial support (START 2014 to M.W.). K.V.H. thanks the Hercules Foundation (project AUGE/11/029 "3D-SPACE: 3D Structural Platform Aiming for Chemical Excellence") and the Special Research Fund (BOF) − UGent (project 01N03217) for funding.

■ DEDICATION

Dedicated to the memory of Prof. Gérard Férey, who passed away on August 19th, 2017.

DOI: 10.1021/acs.cgd.9b00734
Cryst. Growth Des. 2019, 19, 5292−5307

REFERENCES

(1) Haasnoot, J. G. Mononuclear, oligonuclear and polynuclear metal coordination compounds with 1,2,4-triazole derivatives as ligands. *Coord. Chem. Rev.* **2000**, *200–202*, 131–185.

(2) Garcia, Y.; Kahn, O.; Rabardel, L.; Chansou, B.; Salmon, L.; Tuchagues, J. –P. Two-Step Spin Conversion for the Three-Dimensional Compound Tris(4,4′-bis-1,2,4-triazole)iron(II) Diperchlorate. *Inorg. Chem.* **1999**, *38*, 4663–4670.

(3) Huang, Y. – Q.; Zhao, X. – Q.; Shi, W.; Liu, W. – Y.; Chen, Z. – L.; Cheng, P.; Liao, D. – Z.; Yan, S.-P. Anions-Directed Metal-Mediated Assemblies of Coordination Polymers Based on the Bis(4,4′-bis-1,2,4-triazole) Ligand. *Cryst. Growth Des.* **2008**, *8*, 3652–3660.

(4) Deng, Y.; Liu, H.; Yu, B.; Yao, M. Supramolecular Coordination Assemblies Constructed From Multifunctional Azole-Containing Carboxylic Acids. *Molecules* **2010**, *15*, 3478–3506.

(5) Naik, A. D.; Dîrtu, M. M.; Railliet, A. P.; Marchand-Brynaert, J.; Garcia, Y. Coordination *polymers* and metal organic frameworks derived from 1,2,4-triazole amino acid linkers. *Polymers* **2011**, *3*, 1750.

(6) Bai, S. – Q.; Young, D. J.; Andy Hor, T. S. Nitrogen-Rich Azoles as Ligand Spacers in Coordination Polymers. *Chem. - Asian J.* **2011**, *6*, 292.

(7) Aromi, G.; Barrios, L. A.; Roubeau, O.; Gamez, P. Triazoles and tetrazoles: Prime ligands to generate remarkable coordination materials. *Coord. Chem. Rev.* **2011**, *255*, 485–546.

(8) Zhang, J. – P.; Zhang, Y. – B.; Lin, J. – B.; Chen, X.-M. Metal azolate frameworks: from crystal engineering to functional materials. *Chem. Rev.* **2012**, *112*, 1001.

(9) Boldog, I.; Domasevitch, K.; MacLaren, J. K.; Heering, C.; Makhloufi, G.; Janiak, C. A fluorite isoreticular series of porous framework complexes with tetrahedral ligands: new opportunities for azolate PCPs. *CrystEngComm* **2014**, *16*, 148–151.

(10) Heering, C.; Boldog, I.; Vasylyeva, V.; Sanchiz, J.; Janiak, C. *Bifunctional pyrazolate–carboxylate ligands* for *isoreticular cobalt* and *zinc MOF-5 analogs* with *magnetic analysis* of the {*Co4*(*μ4-O*)} *node*. *CrystEngComm* **2013**, *15*, 9757–9768.

(11) Liu, S. – Y.; Zhang, J. – P.; Chen, X.-M. Cu(I) 3,5-Diethyl-1,2,4-Triazolate (MAF-2): From Crystal Engineering to Multifunctional Materials. *Cryst. Growth Des.* **2017**, *17*, 1441–1449.

(12) Li, X.; Yu, Z.; Guan, T.; Li, X.; Ma, G.; Guo, X. Substituent Effects of Isophtalate Derivatives on the Construction of Zinc(II) Coordination Polymers Incorporating Flexible Bis(imidazolyl) Ligands. *Cryst. Growth Des.* **2015**, *15*, 278–290.

(13) Zhai, Q. – Q.; Wu, X.-Q.; Chen, S. – M.; Lu, C.-Z.; Yang, W.-B. Design of Novel Three-Dimensional Coordination Polymers Based on Triangular Trinuclear Copper 1,2,4-Triazolate Units. *Cryst. Growth Des.* **2006**, *6*, 1393–1398.

(14) Yin, P. – X.; Zhang, J.; Qin, Y. – Y.; Cheng, J. – K.; Lia, Z. – J.; Yao, Y. – G. Role of molar-ratio, temperature and solvent on the Zn/Cd 1,2,4-triazolate system with novel topological architectures. *CrystEngComm* **2011**, *13*, 3536–3544.

(15) Ye, Y.; Zhang, H.; Chen, L.; Chen, S.; Lin, Q.; Wei, F.; Zhang, Z.; Xiang, S. Metal–Organic Framework with Rich Accessible Nitrogen Sites for Highly Efficient CO_2 Capture and Separation. *Inorg. Chem.* **2019**, *58*, 7754–7759.

(16) Lu, Z.; Meng, F.; Du, L.; Jiang, W.; Cao, H.; Duan, J.; Huang, H.; He, H. A Free Tetrazolyl Decorated Metal-Organic Framework Exhibiting High and Selective CO_2 Adsorption. *Inorg. Chem.* **2018**, *57*, 14018–14022.

(17) Adarsh, N. N.; Dîrtu, M. M.; Naik, A. D.; Léonard, A. F.; Campagnol, N.; Robeyns, K.; Snauwaert, J.; Fransaer, J.; Su, B. L.; Garcia, Y. A single-walled metal organic nanotube built from a simple synthon. *Chem. - Eur. J.* **2015**, *21*, 4300–4307.

(18) Tăbăcaru, A.; Pettinari, C.; Galli, S. Coordination polymers and metal-organic frameworks built up with poly(tetrazolate) ligands. *Coord. Chem. Rev.* **2018**, *372*, 1–30.

(19) Lysenko, A. B.; Senchyk, G. A.; Domasevitch, K. V.; Hauser, J.; Fuhrmann, D.; Kobalz, M.; Krautscheid, H.; Neves, P.; Valente, A. A.; Goncalves, I. S. Synthesis and Structural Elucidation of Triazolylmolybdenum(VI) Oxide Hybrids and Their Behavior as Oxidation Catalysts. *Inorg. Chem.* **2015**, *54*, 8327–8338.

(20) Meng, L.; Niu, Z.; Liang, C.; Dong, X.; Kang, L.; Li, G.; Li, C.; Han, Y.; Shi, Z.; Feng, S. Integration of Open Metal Sites and Lewis Basic Sites for Construction of a Cu MOF with a Rare Chiral Oh-type cage for high performance in methane purification. *Chem. - Eur. J.* **2018**, *24*, 13181–13187.

(21) Naik, A. D.; Dîrtu, M. M.; Léonard, A.; Tinant, B.; Marchand-Brynaert, J.; Su, B. L.; Garcia, Y. Engineering Three-Dimensional Chains of Porous Nanoballs from a 1,2,4-Triazole-carboxylate Supramolecular Synthon. *Cryst. Growth Des.* **2010**, *10*, 1798–1807.

(22) Wang, W.; Li, J. – L.; Jiang, C.; Hu, P.; Li, B.; Zhang, T.; Zhou, H. – C. An efficient strategy for improving the luminescent sensing performance of a terbium(III) metal–organic framework towards multiple substances. *Chem. Commun.* **2018**, *54*, 13271–13274.

(23) Boland, Y.; Tinant, B.; Safin, D. A.; Marchand-Brynaert, J.; Clérac, R.; Garcia, Y. A metal–organic framework made of an asymmetric 1,2,4-triazole and tetrazole ligand. *CrystEngComm* **2012**, *14*, 8153–8155.

(24) Garcia, Y.; Bravic, G.; Chasseau, D.; Gieck, C.; Tremel, W.; Gütlich, P. Crystal Structure, Magnetic Properties, and ^{57}Fe Mössbauer Spectroscopy of the Two-Dimensional Coordination Polymers [M-(1,2-bis(1,2,4-triazol-4-yl)ethane)$_2$(NCS)$_2$] (M^{II} = Fe, Co). *Inorg. Chem.* **2005**, *44*, 9723–9730.

(25) Jafari, M.; Amani, V. A new Zn mixed-ligand coordination polymer fiber for solid-phase microextraction of the anticancer drug tamoxifen. *Sep. Sci. Plus* **2018**, *1*, 746–752.

(26) Garcia, Y.; Adarsh, N. N.; Naik, A. D. Crystal engineering of Fe(II) spin crossover coordination polymers derived from triazole or tetrazole ligands. *Chimia* **2013**, *67*, 411–418.

(27) Suárez-García, S.; Adarsh, N. N.; Molnár, G.; Bousseksou, A.; Garcia, Y.; Dîrtu, M. M.; Saiz-Poseu, J.; Robles, R.; Ordejón, P.; Ruiz-Molina, D. Spin-Crossover in an Exfoliated 2D Coordination Polymer and Its Implementation in Thermochromic Films. *ACS Appl. Nano Mater.* **2018**, *1*, 2662–2668.

(28) Garcia, Y.; van Koningsbruggen, P. J.; Kooijman, H.; Spek, A. L.; Haasnoot, J. G.; Kahn, O. Synthesis, crystal structure, spectroscopic and magnetic properties of an unprecedented tridimensional Cu(II) coordination compound of 1,2-bis(1,2,4-triazol-4-yl)ethane. *Eur. J. Inorg. Chem.* **2000**, *2000*, 307–314. See also p 575.

(29) Habib, H. A.; Hoffmann, A.; Höppe, H. A.; Steinfeld, G.; Janiak, C. Crystal Structure Solid-State Cross Polarization Magic Angle Spinning ^{13}C NMR Correlation in luminescent d^{10} Metal-Organic Frameworks Constructed with the 1,2-Bis(1,2,4-triazol-4-yl)ethane Ligand. *Inorg. Chem.* **2009**, *48*, 2166–2180.

(30) Liu, X. – G.; Wang, L. – Y.; Zhu, X.; Li, B. – L.; Zhang, Y. Structural Versatility of Eight Zinc(II) Coordination Polymers Constructed with a Long Flexible Ligand 1,4-Bis(1,2,4-triazol-1-yl)butane. *Cryst. Growth Des.* **2009**, *9*, 3997–4005.

(31) El-Massaoudi, M.; Radi, S.; Salhi, A.; Mabkhot, Y. N.; Al-Showiman, S. S.; Ghabbour, H. A.; Adarsh, N. N.; Garcia, Y. Novel 1D Coordination Polymers Built from Acyclic Cryptate Containing bis(1H-1,2,4-triazole) Ligands featuring Coordinated Counteranions. *New J. Chem.* **2018**, *42*, 11324–11333.

(32) Adarsh, N. N.; Dîrtu, M. M.; Guionneau, P.; Devlin, E.; Sanakis, Y.; Howard, J. A. K.; Chattopadhyay, B.; Garcia, Y. One-Dimensional Looped Chain and Two-Dimensional Square Grid Coordination Polymers: Encapsulation of Bis(1,2,4-Triazole)-trans-cyclohexane into the Voids. *Eur. J. Inorg. Chem.* **2019**, *2019*, 585–591.

(33) Naik, A. D.; Marchand-Brynaert, J.; Garcia, Y. A Simplified Approach to N- and N,N′-Linked 1,2,4-Triazoles by Transamination. *Synthesis* **2008**, *2008*, 149–154.

(34) Garcia, Y.; Robert, F.; Naik, A. D.; Zhou, G.; Tinant, B.; Robeyns, K.; Michotte, S.; Piraux, L. Spin Transition Charted in a Fluorophore-Tagged Thermochromic Dinuclear Iron(II) Complex. *J. Am. Chem. Soc.* **2011**, *133*, 15850.

(35) Liu, B.; Bai, L.; Lin, X.; Li, K.; Huan, H.; Hui, H.; Hu, H.; Liu, Y.; Kang, Z. Crystal engineering towards the luminescence property trimming of hybrid coordination polymers. *CrystEngComm* **2015**, *17*, 1686–1692.

DOI: 10.1021/acs.cgd.9b00734
Cryst. Growth Des. 2019, 19, 5292–5307

(36) Benaicha, B.; Van Do, K.; Yangui, A.; Pittala, N.; Lusson, A.; Sy, M.; Bouchez, G.; Fourati, H.; Gómez-García, C. J.; Triki, S.; Boukheddaden, K. Interplay between spin-crossover and luminescence in a multifunctional single crystal iron(II) complex: towards a new generation of molecular sensors. *Chem. Sci.* **2019**, *10*, 6791.
(37) Addison, A. W.; Rao, T. N.; Reedijk, J.; van Rijn, J.; Verschoor, G. C. Synthesis, structure, and spectroscopic properties of copper(II) compounds containing nitrogen−sulphur donor ligands; the crystal and molecular structure of aqua[1,7-bis(N-methylbenzimidazol-2′-yl)-2,6-dithiaheptane]copper(II) perchlorate. *J. Chem. Soc., Dalton Trans.* **1984**, *7*, 1349−1356.
(38) Blatov, V. A.; Shevchenko, A. P.; Proserpio, D. M. Applied Topological Analysis of Crystal Structures with the Program Package ToposPro. *Cryst. Growth Des.* **2014**, *14*, 3576−3586.
(39) Groom, C. R.; Bruno, I. J.; Lightfoot, M. P.; Ward, S. C. The Cambridge Structural Database. *Acta Crystallogr., Sect. B: Struct. Sci., Cryst. Eng. Mater.* **2016**, *B72*, 171−179.
(40) Spek, A. L. Structure validation in chemical crystallography. *Acta Crystallogr., Sect. D: Biol. Crystallogr.* **2009**, *D65*, 148−155.
(41) Marchivie, M.; Guionneau, P.; Letard, J. F.; Chasseau, D. Photo-induced spin-transition: the role of the iron(II) environment distortion. *Acta Crystallogr., Sect. B: Struct. Sci.* **2005**, *61*, 25−28.
(42) Beitat, A.; Foxon, S. P.; Brombach, C. − C.; Hausmann, H.; Heinemann, F. W.; Hampel, F.; Monkowius, U.; Hirtenlehner, C.; Knör, G.; Schindler, S. Syntheses, emission properties and intra-molecular ligand exchange of zinc complexes with ligands belonging to the tmpa family. *Dalton Trans.* **2011**, *40*, 5090−5101.
(43) Yang, Y.; Du, P.; Liu, Y.-Y.; Ma, J.-F. A Series of Coordination Polymers Constructed by Flexible 4-Substituted Bis(1,2,4-triazole) Ligands and Polycarboxylate Anions: Syntheses, Structures, and Photoluminescent Properties. *Cryst. Growth Des.* **2013**, *13*, 4781−4795.
(44) Barbieri, A.; Accorsia, G.; Armaroli, N. Luminescent complexes beyond the platinum group: the d10 avenue. *Chem. Commun.* **2008**, 2185−2193.
(45) Grabowski, Z. R.; Rotkiewicz, K.; Rettig, W. Structural Changes Accompanying Intramolecular Electron Transfer: Focus on Twisted Intramolecular Charge-Transfer States and Structures. *Chem. Rev.* **2003**, *103*, 3899−4032.
(46) Rettig, W. Population of excited charge transfer states and molecular conformation in *N*-phenylpyrrole. *Nouv. J. Chim.* **1983**, *7*, 425−431.
(47) Sarkar, A.; Chakravorti, S. A study on the spectroscopy and photophysics of N-phenyl pyrrole and N-phenyl pyrazole. *Chem. Phys. Lett.* **1995**, *235*, 195−201.
(48) Yoshihara, T.; Druzhinin, S. I.; Demeter, A.; Kocher, N.; Stalke, D.; Zachariasse, K. A. Kinetics of Intramolecular Charge Transfer with N-Phenylpyrrole in Alkyl Cyanides. *J. Phys. Chem. A* **2005**, *109*, 1497−1509.
(49) Yamaji, M.; Kato, S.; Tomonari, K.; Mamiya, M.; Goto, K.; Okamoto, H.; Nakamura, Y.; Tani, F. Blue Fluorescence from BF2 Complexes of N,O-Benzamide Ligands: Synthesis, Structure, and Photophysical Properties. *Inorg. Chem.* **2017**, *56*, 12514−12519.
(50) Vogler, A.; Kunkely, H. Ligand-to-ligand and intraligand charge transfer and their relation to charge transfer interactions in organic zwitterions. *Coord. Chem. Rev.* **2007**, *251*, 577−583.
(51) Sheridan, U.; Gallagher, J. F.; Philippidis, A.; McGinley, J. Zinc complexes of pyridyl-tetrazole derivatives − Highly fluorescent materials. *Inorg. Chim. Acta* **2015**, *432*, 50−55.
(52) Stufkens, D. J.; Vlček, A., Jr. Excited states of metal-metal bonded diimine complexes vary from extremely long lived to very reactive with formation of radicals or zwitterions. *Coord. Chem. Rev.* **1998**, *171*, 93−105.
(53) Xu, Y. Y.; Wu, X. X.; Wang, Y. Y.; Su, X. M.; Liu, S. X.; Zhu, Z. Z.; Ding, B.; Wang, Y.; Huoab, J. Z.; Duab, G. X. Six Zn(II) and Cd(II) coordination polymers assembled from a similar binuclear building unit: tunable structures and luminescence properties. *RSC Adv.* **2014**, *4*, 25172−25182.
(54) Campagnol, N.; Van Assche, T.; Boudewijns, T.; Denayer, J. F. M.; Binnemans, K.; De Vos, D. E.; Fransaer, J. High pressure, high temperature electrochemical synthesis of metal−organic frameworks: films of MIL-100 (Fe) and HKUST-1 in different morphology. *J. Mater. Chem. A* **2013**, *1*, 5827−5830.
(55) Mueller, U. Method for Electrochemical Production of a Crystalline Porous Metal Organic Skeleton Material, 2007, US Patent 2007/0227898 A1.
(56) Mueller, U. Metal−organic frameworks—prospective industrial applications. *J. Mater. Chem.* **2006**, *16*, 626−636.
(57) Hoppe, B.; Hindricks, K. D.; Warwas, D. P.; Schulze, H. A.; Mohmeyer, A.; Pinkvos, T. J.; Zailskas, S.; Krey, M. R.; Belke, C.; König, S.; Fröba, M.; Haug, R. J.; Behrens, P. Graphene-like metal−organic frameworks: morphology control, optimization of thin film electrical conductivity and fast sensing applications. *CrystEngComm* **2018**, *20*, 6458−6471.
(58) Liu, K.; Shia, W.; Cheng, P. The coordination chemistry of Zn(II), Cd(II) and Hg(II) complexes with 1,2,4-triazole derivatives. *Dalton Trans.* **2011**, *40*, 8475−8490.
(59) Yang, L.; Powell, D. R.; Houser, R. P. Structural variation in copper(I) complexes with pyridylmethylamide ligands: structural analysis with a new four-coordinate geometry index, $\tau 4$. *Dalton Trans.* **2007**, 955−964.
(60) Wang, N.; Chao Feng, Y.-C.; Shi, W.; Zhao, B.; Cheng, P.; Liao, D.-Z.; Yana, S.-P. Synthesis, structure, fluorescent and magnetic properties of a series of coordination polymers based on a long and flexible bis-triazole ligand. *CrystEngComm* **2012**, *14*, 2769−2778.
(61) *CrysAlisPro Software system, Version 1.171.37.35*; Rigaku Corporation: Oxford, UK, 2018.
(62) Sheldrick, G. M. SHELXT - Integrated space-group and crystal-structure determination. *Acta Crystallogr., Sect. A: Found. Adv.* **2015**, *A71*, 3−8.
(63) Macrae, C. F.; Edgington, P. R.; McCabe, P.; Pidcock, E.; Shields, G. P.; Taylor, R.; Towler, M.; Van De Streek, J. Mercury: visualization and analysis of crystal structures. *J. Appl. Crystallogr.* **2006**, *39*, 453−457.
(64) Dolomanov, O. V.; Bourhis, L. J.; Gildea, R. J.; Howard, J. A. K.; Puschmann, H. OLEX2: a complete structure solution, refinement and analysis program. *J. Appl. Crystallogr.* **2009**, *42*, 339−341.
(65) Sheldrick, G. M. A short history of *SHELX*. *Acta Crystallogr., Sect. A: Found. Crystallogr.* **2008**, *64*, 112−122.

DOI: 10.1021/acs.cgd.9b00734
Cryst. Growth Des. 2019, 19, 5292−5307